UNIVERSIDADE FEDERAL DE SÃO CARLOS

CENTRO DE CIÊNCIAS BIOLÓGICAS E DA SAÚDE

PROGRAMA DE PÓS-GRADUAÇÃO EM CIÊNCIAS AMBIENTAIS

ELTON VICENTE ESCOBAR SILVA

MODELO DE CRESCIMENTO DE GRAMÍNEAS ADAPTADO A ÁREAS URBANAS

São Carlos
[2019]

ELTON VICENTE ESCOBAR SILVA

MODELO DE CRESCIMENTO DE GRAMÍNEAS ADAPTADO A ÁREAS URBANAS

Dissertação apresentada ao Programa de Pós-Graduação em Ciências Ambientais da Universidade Federal de São Carlos, como parte dos requisitos para a obtenção do título de Mestre em Ciências Ambientais[1].

Orientação: Prof. Dr. Vandoir Bourscheidt

São Carlos
[2019]

UNIVERSIDADE FEDERAL DE SÃO CARLOS

Centro de Ciências Biológicas e da Saúde
Programa de Pós-Graduação em Ciências Ambientais

Folha de Aprovação

Assinaturas dos membros da comissão examinadora que avaliou e aprovou a Defesa de Dissertação de Mestrado do candidato Elton Vicente Escobar Silva, realizada em 09/09/2019:

Prof. Dr. Vandoir Bourscheidt
UFSCar

Prof. Dr. José Ricardo Macedo Pezzopane
EMBRAPA

Prof. Dr. Camilo Daleles Rennó
INPE

Certifico que a defesa realizou-se com a participação à distância do(s) membro(s) Camilo Daleles Rennó e, depois das arguições e deliberações realizadas, o(s) participante(s) à distância está(ao) de acordo com o conteúdo do parecer da banca examinadora redigido neste relatório de defesa.

Prof. Dr. Vandoir Bourscheidt

DEDICATÓRIA

Á minha querida mãe por sempre
acreditar em minhas capacidades, muita
vezes, mais do que eu mesmo. E ao meu
saudoso pai (*in memoriam*).

AGRADECIMENTOS

À minha mãe, Beth, por todo carinho, paciência, compreensão, inúmeros sacrifícios e apoio incondicional. Por ser exemplo de pessoa e me ensinar os valores que carrego hoje. Agradeço também a todo suporte de minha família, que foi o alicerce dessa minha caminhada.

Ao meu orientador, Prof. Dr. Vandoir Bourscheidt, pela oportunidade de realizar esse projeto. Agradeço-o também pelas inúmeras conversas, orientações, auxílios, paciência e por estar presente em todos os momentos decisivos, inclusive no meu período de intercâmbio. O meu sincero muito obrigado.

Ao meu orientador de intercâmbio, Dr. Craig S. T. Daughtry, pela oportunidade única de estagiar no laboratório de Sensoriamento Remoto e Hidrologia do Departamento de Agricultura dos Estados Unidos (USDA–ARS) e por todo compartilhamento de conhecimento. Também agradeço aos pesquisadores Dr. Dennis J. Timlin, Dr. David H. Fleisher, Dr. James R. Kiniry, do USDA, e ao Prof. Dr. André Backes da Universidade Federal de Uberlândia (UFU), pelas contribuições científicas a esse trabalho.

Aos amigos e amigas de departamento por todos os momentos alegres e descontraídos vivenciados que me motivaram a seguir em frente e nunca desistir.

Enfim, a todos aqueles que contribuíram diretamente e indiretamente para o meu processo de aprendizagem e para a realização dessa etapa tão significante em minha vida.

EPÍGRAFE

"Knowing how to think
empowers you far beyond those
who know only what to think."

Neil deGrasse Tyson

Escobar-Silva, E. V. Modelo de crescimento de gramíneas adaptado a áreas urbanas. 2019 – 94p: Dissertação (Mestrado) – Universidade Federal de São Carlos, Centro de Ciências Biológicas e da Saúde, Programa de Pós-Graduação em Ciências Ambientais, São Carlos – 2019.

RESUMO:

A existência de espaços verdes em áreas urbanas e seus impactos na população têm sido objeto de muitos estudos, não apenas pelos importantes serviços ecossistêmicos prestados por essas áreas, mas também pela contribuição direta na saúde pública. Iniciativas para o controle da vegetação urbana, quanto à otimização do processo de corte/roçada, redução de custos e, potencialmente, redução de impactos no ecossistema natural urbano, não foram encontradas na literatura. Assim, este trabalho visa implementar um modelo de crescimento de gramíneas ajustado para o manejo adequado de áreas verdes urbanas, especificamente parques e praças públicas, e o entorno de ruas, estradas e corpos d'água. O modelo foi desenvolvido em Python e simula a dinâmica diária do índice de área foliar (IAF), biomassa, evapotranspiração e teor de água no solo, passando por processos de corte ou não, com configurações para a espacialização das informações e eventual inclusão em sistemas de informação geográfica (SIG). Entretanto, apenas o crescimento acima do solo é modelado. Teor de água no solo, temperatura e radiação são considerados as únicas limitações ao crescimento da planta. O modelo apresenta dois estágios de desenvolvimento para a planta, ciclo de crescimento e dormência. O período de dormência pode ser iniciado a partir de duas abordagens diferentes: duração do dia ou índice de umidade do solo - SMI, o que permite cobrir áreas temperadas e tropicais. É apresentado um estudo de caso utilizando a grama batatais (*Paspalum notatum* Flügge) como espécie de interesse para a execução do modelo, bem como os procedimentos de avaliação do desempenho do mesmo. Duas plataformas diferentes (um veículo aéreo não tripulado - imagens UAV e PlanetScope) foram utilizadas na aquisição de dados e os índices de vegetação NDVI, GNDI e EVI2 foram usados para recuperar o IAF a partir de medições *in situ* e dos sensores. O EVI2 apresentou o melhor desempenho para a recuperação do IAF da grama batatais e, portanto, foi utilizado na avaliação do IAF simulado no modelo. Para avaliar o desempenho do modelo, foi realizada uma comparação entre o IAF do modelo (default e ajustado) e IAF recuperados de ambos os sensores, adotando como critério de analise o coeficiente de determinação associado (R^2) e a raiz do erro quadrático médio (RMSE). Os resultados obtidos na análise sugerem que o modelo proposto é adequado à sua finalidade, e, sua eventual utilização pode auxiliar as

administrações governamentais na otimização dos processos de corte/roça das áreas verdes urbanas. Entretanto, alguns ajustes no desenvolvimento da curva LAI e no período de dormência ainda são sugeridos.

Palavras-chave: Modelo de crescimento de gramíneas; Áreas urbanas; SIG.

ABSTRACT

Green spaces in urban areas and its impacts on the population has been the subject of many studies, not only because of the important ecosystem services provided by these areas but also due to the direct contribution on public health. Initiatives for control of urban vegetation, regarding the optimization of the mowing process, reducing costs and potentially reducing impacts on the urban natural ecosystem have not been found in the literature. Thus, this work aims to implement a grass growth model suitable for appropriate management of urban green spaces, specifically in lawns, public parks squares, roadsides and around waterways. The model was developed in Python and simulates the daily dynamics of leaf area index (LAI), biomass, evapotranspiration and soil water content, going under mowing processes or not, with spatialization capability which might be integrated within geographic information system (GIS) environment. However, only above-ground growth is modeled. Soil water content, temperature, and radiation stress are considered the only environmental growth limitations. The model presents two development stages for the plant, growth cycle and dormancy. The dormant period can be trigged from two different approaches: daylength or the soil moisture index - SMI, which allows covering temperate and tropical areas. A case study using bahiagrass (*Paspalum notatum* Flügge) as input to run the model is presented as well as the evaluation procedures of the model performance. Two different platforms (an unmanned aerial vehicle – UAV and PlanetScope imagery) were used in the data acquisition and, the vegetation indices NDVI, GNDI, and EVI2 were used to retrieve LAI from *in situ* measurements and from the sensors. EVI2 showed the best performance for bahiagrass LAI retrieval and thus it was used in the evaluation of the LAI simulated in the model. To assess the performance of the model, LAI from the model (default and adjusted) and LAI retrieved from both sensors are compared using the associated determination coefficient (R^2) and root mean square error (RMSE) as criteria. The results obtained in the analysis suggest that the proposed model is suitable for its purpose and its eventual application may help government administrations with the optimization of mowing processes of urban green spaces (UGS). However, some adjustments in the LAI curve development and in the dormant period are suggested.

Keywords: Grass growth model; Urban area; GIS.

LISTA DE FIGURAS

LISTA DE TABELA E QUADROS

ACRONYMS

APAR	Absorbed photosynthetically active radiation
ASD	Analytical spectral device
DEM	Digital Elevation Model
DOY	Day of year
DSM	Digital Surface Model
EF	Environmental factor
EPIC	Environmental Policy Integrated Climate
ET_o	Reference evapotranspiration
EVI2	Two-band enhanced vegetation index
GIS	Geographic information systems
GNDVI	Green normalized difference vegetation index
HAND	Height Above the Nearest Drainage
HU	Heat unit
HUI	Heat unit index
K_s	Water stress coefficient
LAI	Leaf area index
NDVI	Normalized difference vegetation index
NIR	Near-infrared
P	Precipitation
PAR	Photosynthetically Active Radiation
PHU	Potential heat units
R^2	Coefficient of determination
Rad_{str}	Radiation stress
SMI	Soil moisture index
SRTM	Shuttle Radar Topography Mission
T	Temperature
T_{str}	Temperature stress
UGS	Urban green spaces
UN	The United Nations
VIs	Vegetation indices
W_{str}	Soil water stress

SUMÁRIO

ESTRUTURA DA DISSERTAÇÃO

A dissertação foi elaborada no formato de artigos científicos. Os artigos são antecedidos por uma introdução geral que visa contextualizar a temática do trabalho e, em seguida, são apresentados os objetivos gerais e específicos que orientam este trabalho.

O primeiro artigo, "*A GRASS GROWTH MODEL ADAPTED TO URBAN AREAS. PART 1: MODEL DESCRIPTION*", teve como objetivo a implementação de um modelo de crescimento de gramíneas adaptado para áreas urbanas. O modelo apresentado neste trabalho foi estruturado a partir de componentes de modelos agrometeorológicos pré-existentes.

O segundo artigo, *"A GRASS GROWTH MODEL ADAPTED TO URBAN AREAS. PART 2: MODEL PERFORMANCE ASSESS BY COMPARISON BETWEEN SIMULATED LAI AND LAI RETRIEVED FROM VEGETATION INDEX*", descreve o processo de avaliação do desempenho do modelo. Essa avaliação foi feita a partir da comparação do índice de área foliar (IAF) simulado pelo modelo com IAF recuperado de índice de vegetação (VI) a partir de dados coletados de duas plataformas diferentes, um veículo aéreo não tripulado e satélites de pequeno porte (CubeSats). Para a construção da equação de regressão do IAF a partir de VI, foram coletados reflectância e IAF *in situ* e utilizados como referência.

Subsequente aos artigos, são apresentadas as considerações finais, a conclusão geral da dissertação e recomendações para trabalhos futuros.

1. INTRODUÇÃO

A forma que os aglomerados urbanos e as atividades humanas estão organizadas no espaço geográfico, juntamente com as altas taxas de crescimento da população e da área urbana, representam uma fonte de preocupação para a sociedade moderna, principalmente em termos de impactos socioambientais (CAMAGNI, CAPELLO, NIJKAMP, 1998; BUCK, MARIN, 2005). Ao longo da história, os modelos de infraestrutura dos assentamentos urbanos eram caracterizados por áreas compactas, com alta densidade populacional e lenta taxa de expansão, mas esse cenário tem mudado nas últimas décadas (SETO, SANCHEZ-RODRIGUEZ, FRAGKIAS, 2010), sendo que atualmente a taxa de expansão urbana é em média duas vezes maior do que o seu crescimento populacional (ANGEL et al., 2011; SETO et al., 2011).

De acordo com o relatório da Organização das Nações Unidas – ONU (UN, 2017) sobre as perspectivas do mundo globalizado, a população mundial, no ano de 2017, era próxima de 7,6 bilhões de pessoas e com taxa de crescimento anual de 1,10%. Assim, segundo as projeções da ONU, é estimado que para o ano de 2030 a população mundial chegue a 8,6 bilhões de pessoas, e que ultrapasse 11 bilhões de pessoas em 2100. Já a população urbana mundial, no ano de 2014, era de aproximadamente 3,9 bilhões de pessoas, o que representava 54% da população global (UN, 2015). No cenário brasileiro, a grande expansão urbana é considerada recente, seu início data da década de 1930, mas foi somente a partir da década de 70, do mesmo século, que a população urbana ultrapassou a população rural (BRITO, HORTA, AMARAL, 2001; BRITO, SOUZA, 2005; MARTINE et al., 2016). De acordo com o último censo demográfico realizado pelo Instituto Brasileiro de Geografia e Estatística – IBGE (2010), aproximadamente 161 milhões de pessoas residiam na área urbana, representando 85% da população total.

No ambiente citadino, pode-se afirmar que as condições socioambientais são reflexo das relações intrínsecas existentes entre a dinâmica populacional, suporte físico do ambiente, desenvolvimento e as alterações antrópicas no meio ambiente (SOUSA, TRAVASSOS, 2008; MARTINE, 2007; MARTINE, MCGRANAHAN, 2010). Desta forma, o crescimento acelerado da população urbana poderá comprometer a capacidade dos governos locais de fornecer serviços básicos essenciais para a população, tais como habitação,

eletricidade, água potável, saneamento básico, aplicação da lei e ordem, e desenvolvimento do capital social (BUHAUG, URDAL, 2013). Como possíveis consequências, a qualidade de vida dos cidadãos sofrerá perturbações e problemas socioambientais serão potencializados (HARDOY, MITLIN, SATTERTHWAITE, 2013).

Neste contexto, a existência de espaços verdes em áreas urbanas e seus impactos sobre a população têm sido documentados por diferentes autores (e.g. CHIESURA, 2004; GERMANN-CHIARI, SEELAND, 2004; JENERETTE, 2007; WOLCH, BYRNE, NEWELL 2014). Além dos importantes serviços ambientais fornecidos por essas áreas, tais como purificação da água, do ar, filtragem dos ventos e dos ruídos, e estabilização do microclima, elas contribuem diretamente na saúde pública, pois proporcionam serviços sociais e psicológicos importantes para a manutenção do bem-estar dos seres humanos nos centros urbanos (CHIESURA, 2004; BOLUND, HUNHAMMAR, 1999). Logo, para propiciar qualidade ambiental à população urbana, é fundamental oferecê-la espaços que possibilitem a interação com o ambiente natural, principalmente com a presença de vegetação (BARGOS, MATIAS, 2012).

No aspecto econômico, áreas urbanas com maior concentração de vegetação, apresentam, normalmente, maior valor monetário agregado (LUTTIK, 2000; MORANCHO, 2003; JENERETTE, 2007). Essa tendência é justificada devido à relação positiva entre áreas verdes e qualidade de vida, em termos de conforto, o qual, por sua vez, está associado com fatores fisiológicos (temperatura) e psicológicos (nível de estresse, por exemplo) do ser humano. Dessa forma, essas áreas devem ser compreendidas como ecossistemas complexos e necessitam de maior entendimento para além de simples áreas de recreação (CHIESURA, 2004; GERMANN-CHIARI, SEELAND, 2004; JENERETTE, 2007; WOLCH, BYRNE, NEWELL, 2014).

A mitigação e a solução dos problemas socioambientais urbanos enfrentados pela sociedade moderna passam pela pesquisa, discussão e desenvolvimento do conhecimento científico tecnológico, além da educação ambiental e gestão pública, que devem ser adequadas à realidade local (FRANCISCO, 2005; BARGOS, MATIAS, 2012). Para assegurar condições ambientais que proporcionem qualidade de vida no contexto de crescimento urbano e populacional acelerado em todo o mundo, é importante um entendimento mais aprofundado do

conceito emergente de cidade inteligente (do inglês *Smart City*) (CHOURABI, 2012). Até o momento não existe na literatura uma definição única para esse conceito, mas pode-se dizer que uma cidade inteligente busca o crescimento econômico sustentável e alta qualidade de vida para os seus residentes, com uma gestão sensata dos recursos naturais, por meio da governança participativa, incitadas pelo investimento em capital humano e social, e infraestrutura de comunicação tanto tradicional (transporte) quanto moderna (ICTs - *Information and Communication Technologies*) (CARAGLIU, DEL BO, NIJKAMP, 2011).

Dentre as diversas iniciativas no contexto de implementação de cidades inteligentes, pode-se inserir iniciativas para o controle paisagístico da vegetação urbana, de forma a otimizar o processo de corte (poda), diminuindo os custos e ainda, potencialmente, diminuindo os impactos sobre o ecossistema natural urbano. Estes custos podem variar significativamente entre diferentes regiões e estratos socioeconômicos das cidades e regiões (ESCOBEDO et al., 2006). Entretanto, iniciativas específicas nesta direção não foram encontradas na literatura, sendo as existentes focadas apenas na avaliação da adequabilidade da distribuição espacial dos espaços verdes nas cidades utilizando Sistemas de Informação Geográfica – SIG (OH, JEONG, 2007). Desta forma, esse trabalho visa implementar um modelo de crescimento de gramíneas, o qual poderá ser utilizado como ferramenta para a gestão adequada de áreas verdes urbanas, especificamente gramados, parques e praças públicas, e entornos de corpos d'água e de rodovias.

O trabalho proposto nessa dissertação está dividido em duas partes, a primeira se dá na implementação do modelo de crescimento de gramíneas adaptado para áreas urbanas, utilizando parâmetros de modelos de crescimento de vegetação pré-existentes. O modelo implementado, baseou-se, principalmente, nos componentes presentes em três modelos: EPIC (WILLIAMS et al. 1989), ALMANAC (KINIRY et al., 1992), e o modelo de Jouven (JOUVEN et al., 2006a). Já a segunda parte envolve a avaliação do desempenho do modelo em uma área piloto. Nessa parte, utilizou-se a técnica de recuperação do índice de área foliar (IAF) a partir de índices de vegetação (IV). Para isso, foram coletados dados em *in situ* e de sensores acoplados em diferentes plataformas, por meio de um veículo aéreo não tripulado (VANT) e satélites de pequeno porte. Os valores obtidos a partir da recuperação do IAF foram adotados como referência e confrontados com os valores gerados na simulação do modelo.

Por fim, o monitoramento diário da dinâmica do crescimento da vegetação das áreas urbanas faz-se fundamental para viabilizar a gestão adequada dessas áreas. Assim, o modelo foi desenvolvido para possibilitar sua integração em ambiente SIG, visando facilitar, no futuro, o monitoramento das áreas verdes urbanas pelo poder público e otimizar o sistema de corte.

1.1. OBJETIVO GERAL

A ideia central deste trabalho é implementar um modelo de crescimento de gramíneas adaptado a áreas urbanas e configurado para ser integrado em ambiente SIG. Este trabalho resulta do fato de não terem sido encontradas, na literatura, iniciativas que utilizem modelos computacionais como foco nas variações do crescimento da vegetação em áreas urbanas que, entre outros fatores, são determinadas pelo corte regular.

1.2. OBJETIVOS ESPECÍFICOS

Dentre os objetivos específicos envolvidos no desenvolvimento deste trabalho, pode se destacar:

- Implementação de um modelo de crescimento de gramíneas adaptado as condições urbanas.
- Adaptação do modelo para incorporação do modelo em SIG;
- Avaliação do desempenho do modelo em área piloto a partir a recuperação do IAF por meio de índices de vegetação (do inglês vegetation indices - VIs) obtidos de imagens de sensores acoplados em diferentes plataformas, um veículo aéreo não tripulado – VANT e satélites de pequeno porte.

1.3. REFERÊNCIAS

ANGEL, Shlomo; PARENT, Jason; CIVCO, Daniel L.; BLEI, Alexander; POTERE, David. (2011). The dimensions of global urban expansion: Estimates and projections for all

countries, 2000-2050. Evaluation and Program Planning, nº 75, p.53-107. https://doi.org/10.1016/j.progress.2011.04.001.

BARGOS, Danubia Caporusso; MATIA, Lindon Fonseca. (2012). Mapeamento e análise de áreas verdes urbanas em Paulínia (SP): estudo com a aplicação de geotecnologias. Sociedade & Natureza, v. 24, nº 1, p. 143-156. http://dx.doi.org/10.1590/S1982-45132012000100012.

BOLUND, Per; HUNHAMMAR, Sven. (1999). Ecosystem services in urban areas. Ecological economics, v. 29, nº 2, p. 293-301. https://doi.org/10.1016/S0921-8009(99)00013-0.

BRITO, Fausto; HORTA, Cláudia Júlia Guimarães; AMARAL, Ernesto F. L. (2001). A urbanização recente no Brasil e as aglomerações metropolitanas. In: XXIV IUSSP General Conference, p. 168-184. DOI: 10.31219/osf.io/84b92.

BRITO, Fausto; SOUZA, Joseane de. (2005). Expansão urbana nas grandes metrópoles: o significado das migrações intrametropolitanas e da mobilidade pendular na reprodução da pobreza. São Paulo em Perspectiva, v. 19, n. 4, p. 48-63, out./dez. 2005. http://dx.doi.org/10.1590/S0102-88392005000400003.

BUCK, Sonia; MARIN, Andreia Aparecida. (2005). Educação para pensar questões socioambientais e qualidade de vida. Educar em Revista, (25), 197-212. http://dx.doi.org/10.1590/0104-4060.373.

BUHAUG, Halvard; URDAL, Henrik. (2013). An urbanization bomb? Population growth and social disorder in cities. Global Environmental Change, nº 23.1, 2013, p. 1-10. https://doi.org/10.1016/j.gloenvcha.2012.10.016.

CAMAGNI, Roberto; CAPELLO, Roberta; NIJKAMP, Peter. (1998). Towards Sustainable City Policy: an Economy-Environment-Technology nexus. Ecological Economics, nº 24, p.103–118. https://doi.org/10.1016/S0921-8009(97)00032-3.

CARAGLIU, Andrea; DEL BO, Chiara; NIJKAMP, Peter. (2011). Smart cities in Europe. Journal of urban technology, v. 18, nº. 2, p. 65-82. https://doi.org/10.1080/10630732.2011.601117.

CHIESURA, Anna. (2004). The role of urban parks for the sustainable city. Landscape and urban planning, v. 68, n. 1, p. 129-138. https://doi.org/10.1016/j.landurbplan.2003.08.003.

CHOURABI, Hafedh; NAM, Taewoo; WALKER, Shawn; GIL-GARCIA, J. Ramon; MELLOULI, Sehl; NAHON, Karine; PARDO, Theresa A.; SCHOLL, Hans Jochen. (2012). Understanding smart cities: An integrative framework. In: System Science (HICSS), 45th Hawaii International Conference on System Sciences. IEEE, p. 2289-2297. DOI: 10.1109/HICSS.2012.615.

ESCOBEDO, Francisco J.; NOWAK, David J.; WAGNER, John E.; MAZA, Carmen Luz de la; RODRÍGUEZ, Manuel; CRANE, Daniel E.; HERNÁNDEZ, Jaime. (2006). The socioeconomics and management of Santiago de Chile's public urban forests. Urban Forestry & Urban Greening, v. 4, n. 3, p. 105-114. https://doi.org/10.1016/j.ufug.2005.12.002.

FRANCISCO, Denise Pinheiro. (2005). Danos socioambientais urbanos em Curitiba: uma abordagem geográfica. Revista Ra'e Ga - O Espaço Geográfico em Análise, n. 9, p. 47-58. http://dx.doi.org/10.5380/raega.v9i0.3446.

GERMANN-CHIARI, Christina; SEELAND, Klaus. (2004). Are urban green spaces optimally distributed to act as places for social integration? Results of a geographical information

system (GIS) approach for urban forestry research. Forest Policy and Economics, v. 6, n. 1, p. 3-13. https://doi.org/10.1016/S1389-9341(02)00067-9.

HARDOY, Jorge E.; MITLIN, Diana; SATTERTHWAITE, David. (2013). Environmental problems in an urbanizing world: finding solutions in cities in Africa, Asia and Latin America. Routledge, p. 464. https://doi.org/10.4324/9781315071732.

INSTITUTO BRASILEIRO DE GEOGRAFIA E ESTATÍSTICA – IBGE. (2010). Censo Demográfico - 2010: Características da população e dos domicílios: resultados do universo. Rio de Janeiro: IBGE, 2010. Disponível em: <http://www.ibge.gov.br/home/estatistica/populacao/censo2010/caracteristicas_da_popul acao/caracteristicas_da_populacao_tab_pdf.shtm > Acesso em: jul. 2017.

JENERETTE, G. Darrel; HARLAN, Sharon L.; BRAZEL, Anthony; JONES, Nancy; LARSEN, Larissa; STEFANOV, William L. (2007). Regional relationships between surface temperature, vegetation, and human settlement in a rapidly urbanizing ecosystem. Landscape Ecology, v. 22, n. 3, p. 353-365. https://doi.org/10.1007/s10980-006-9032-z.

JOUVEN, M.; CARRÈRE, P.; BAUMONT, R. (2006a). Model predicting dynamics of biomass, structure and digestibility of herbage in managed permanent pastures. 1. Model description. Grass Forage Sci. 61 (2), 112–124. https://doi.org/10.1111/j.1365-2494.2006.00515.x.

KINIRY, J. R., BURSON, B. L.; EVERS, G. W.; WILLIAMS, J. R.; SANCHEZ, H.; WADE, C.; FEATHERSTON, J. W.; GREENWADE, J. (2007). Coastal bermudagrass, bahiagrass, and native range simulation at diverse sites in Texas. Agronomy Journal 99, no. 2, 2007: 450-461. https://doi.org/10.2134/agronj2006.0119.

LUTTIK, Joke. (2000). The value of trees, water and open space as reflected by house prices in the Netherlands. Landscape and urban planning, 48(3-4), 161-167. https://doi.org/10.1016/S0169-2046(00)00039-6.

MARTINE, George. (2007). O lugar do espaço na equação população/meio ambiente. Revista Brasileira de Estudos de População, v. 24, nº 2, p.181-190. http://dx.doi.org/10.1590/S0102-30982007000200002.

MARTINE, George; CAMARANO, Ana Amélia; NEUPERT, Ricardo; BELTRÃO, Kaisô. (2016). A urbanização no Brasil: retrospectiva, componentes e perspectivas. Anais, (VI), 2016, p. 19-65. Disponível em: <http://www.abep.org.br/publicacoes/index.php/anais/article/view/456> Acesso em: 29 . 2017.

MARTINE, George; MCGRANAHAN, Gordon. (2010). A transição urbana brasileira: trajetória, dificuldades e lições aprendidas. População e Cidades: subsídios para o planejamento e para as políticas sociais. Brasília: UNFPA, 2010, p. 11-24. Disponível em: < http://www.unfpa.org.br/Arquivos/populacao_cidade.pdf#page=12> Acesso em: 01 ago. 2017.

MORANCHO, Aurelia Bengochea. (2003). A hedonic valuation of urban green areas. Landscape and urban planning, 66(1), 35-41. https://doi.org/10.1016/S0169-2046(03)00093-8.

OH, Kyushik; JEONG, Seunghyun. (2007). Assessing the spatial distribution of urban parks using GIS. Landscape and urban planning, v. 82, n. 1, p. 25-32. https://doi.org/10.1016/j.landurbplan.2007.01.014.

SETO, Karen C.; SANCHEZ-RODRIGUEZ, Roberto; FRAGKIAS, Michail. (2010). The new geography of contemporary urbanization and the environment. Annual Review of Environment and Resources, nº 35, 2010, p.167–194. https://doi.org/10.1146/annurev-environ-100809-125336.

SETO, Karen C.; FRAGKIAS, Michail; GÜNERALP, Burak; REILLY, Michael K. A meta-analysis of global urban land expansion. PLoS ONE 6:e23777. 2011. https://doi.org/10.1371/journal.pone.0023777.

SOUSA, Lucia; TRAVASSOS, Luciana. (2008). Problemas ambientais urbanos: desafios para a elaboração de políticas públicas integradas. Cadernos Metrópole, nº 19, 2008, p. 27-47. https://doi.org/10.1590/8708.

UNITED NATIONS – UN, Department of Economic and Social Affairs, Population Division. World Urbanization Prospects: The 2014 Revision, 493p. 2015. Disponível em <https://esa.un.org/unpd/wup/Publications/Files/WUP2014-Report.pdf> Acesso em: 14 set. 2017.

UNITED NATIONS – UN, Department of Economic and Social Affairs, Population Division World Population Prospects: The 2017 Revision, Key Findings and Advance Tables. Working Paper No. ESA/P/WP/248. 2017. Disponível em <https://esa.un.org/unpd/wpp/Publications/Files/WPP2017_KeyFindings.pdf> Acesso em: 02 ago. 2017.

WILLIAMS, J. R.; JONES, C. A.; KINIRY, J. R.; SPANEL, D. A. (1989). The EPIC crop growth model. Transactions of the ASAE, 32(2), 497-0511. https://doi.org/10.13031/2013.31032.

WOLCH, Jennifer R.; BYRNE, Jason; NEWELL, Joshua P. (2014). Urban green space, public health, and environmental justice: The challenge of making cities 'just green enough'. Landscape and Urban Planning, v. 125, p. 234-244, 2014. https://doi.org/10.1016/j.landurbplan.2014.01.017.

2. A GRASS GROWTH MODEL ADAPTED TO URBAN AREAS. PART 1: MODEL DESCRIPTION

2.1. ABSTRACT

In Brazil, grass species are widely grown in urban public areas, specifically in lawns, public parks squares, roadsides and around waterways. However, grass growth is often highly complex to predict. In this context, this work is intended to implement a grass growth model adapted to urban areas based on models already developed. The model was developed in Python and is designed to simulate the daily dynamics of leaf area index (LAI), biomass, evapotranspiration and soil water content, from local to large scales, going under mowing processes or not, in geographic information system (GIS) environment. However, only above-ground growth is modeled. Water, temperature, and radiation stress are considered the only environmental growth limitations since there are no records of the nutrient content in urban area soils. The model presents two development stages for the plant, growth cycle and dormancy. The dormant period threshold is based on two different approaches: daylength or the soil moisture index - SMI, which allow covering both temperate and tropical areas. During dormancy, a function with a sigmoidal decrease of LAI toward a minimum value (defined by the user) is applied. Lastly, a case study using bahiagrass (*Paspalum notatum* Flügge) as input to run the model is presented. The results obtained in the analysis suggest that the proposed model is suitable for its purpose and it may be considered an important tool for grass mowing process of urban green spaces (UGS).

Keywords: grass growth; model; urban area.

2.2. INTRODUCTION

According to the United Nations – UN (2015), more than half of world's population lives in cities (approximately 3.9 billion people), and urban population numbers will continue to increase. The UN projects nearly 5.1 billion urban inhabitants by 2030, which represents an increase of 30% (UN, 2015). Thus, this expected urban population growth and its resulting urban sprawl and densification, especially in developing countries, presents an

enormous challenge for sustainable urban planning and management, and subsequently for human health and well-being.

Directly or indirectly, urbanization may lead to problems such as environmental pollution, heat island effects, climate change, among others (McMichael, 2000). On the other hand, several scientific studies have suggested that urban green spaces – UGS (such as public parks, greenways, street trees, edges of roads, railways and waterways, public and private gardens, as well as remnant patches of natural vegetation) provides a wide range of environmental and social benefits (MAAS et al, 2006; BOWLER et al., 2010; WOLCH, BYRNE, NEWELL, 2014; BERTRAM, REHDANZ, 2015). These benefits are not only important for supporting the ecological integrity of cities but also to increase the citizens' quality of life (BOLUND, HUNHAMMAR, 1999; PAULEIT, DUHME, 2000; TZOULAS et al., 2007; HAQ, 2011, WOLCH, BYRNE, NEWELL, 2014).

As environmental benefits, UGS may filter air, remove or reduce pollution, attenuate noise, cool temperatures, infiltrate rainfall water, and replenish groundwater (BOLUND, HUNHAMMAR, 1999; NOWAK, CRANE, STEVENS, 2006; LAFORTEZZA et al., 2009; BOWLER et al., 2010). The social benefits for urban residents include improvements in mental and physical health such as stress reduction and relaxation associated with exposure to UGS (ULRICH, 1983; ULRICH et al., 1991; CHIESURA, 2004; MAAS ET AL, 2006). Furthermore, proximity to public parks and sport fields may increase physical activity levels, which is also important for mental health. (KACZYNSKI, HENDERSON, 2007; WOLCH, BYRNE, NEWELL, 2014). Thus, today's policymakers can no longer ignore the role played by green areas in urban environments (HAQ, 2011; WOLCH, BYRNE, NEWELL, 2014).

Monitoring and modelling of vegetation growth have been the subject of many studies on the field of agriculture, forestry and environmental science (BAIER, 1979; FOURCAUD et al., 2008; PIAO et al., 2011). In this scenario, several statistical approaches and process-based plant models have been developed to simulate plant development and growth, biomass production, and crop yield (ARAUJO, SOUZA, TSUKAHARA, 2011; TAO, YOKOZAWA, ZHANG, 2009; MARCELIS, HEUVELINK, GOUDRIAAN, 1998). However, once plant growth occurs on several scales, ranging from the cellular to the tissue level, its realistically modeling is extremely challenging (CHICKARMANE et al., 2010).

Computational models are powerful tools that not only describe, simulate, analyze, and forecast interactions of complex systems (physical or biological), but also test hypotheses and to improve existing knowledge (LENTZ, 1998; MARCELIS, HEUVELINK, GOUDRIAAN, 1998; CHICKARMANE et al., 2010; DELLA PERUTA, KELLER, SCHULIN, 2014). Furthermore, simulation models provide a suitable way to represent scientific understanding and theory in complex biological systems such as plants and trees (LE ROUX et al., 2001).

Daily or time-steps vegetation models utilize physical and biological functional components to simulate how plants respond to environmental factors (e.g. light, air temperature, soil characteristics, and water availability) and management practices (e.g. sowing date, fertilizer application, harvesting and mowing processes) over time with given genetic traits (MULLER, MARTRE 2019, BOOTE et al., 2013). Moreover, the resulting simulations are used to predict not only temporal changes of the plant but also of its associated variables, such as canopy cover, canopy height, leaf area and biomass produced by the plants, which can be either removed during harvest operations or ends up as surface residue material (ARNOLD et al., 1995).

Agroclimatic models, i.e. models that establish plant-climate relations, can be classified into three categories (BAIER, 1978): i) growth simulation models, defined as a simplified mathematical representation of the complex underlying physical, chemical, and physiological mechanisms to plant growth responses; ii) agrometeorological analysis models, providing a running account of the accumulated (daily) plant responses to selected agrometeorological variables as a function of time (or plant development); iii) empirical-statistical models, in which one or several variables – representing weather or climate, soil characteristics or a time trend – are statistically related mostly to seasonal yield or other plant statistics.

Over the last 50 years, the development of process-based vegetation models has advanced considerably and nowadays there are several of them, which present different degrees of complexity depending on their application (FOURCAUD et al., 2008; MULLER, MARTRE 2019). Agricultural Land Management Alternative with Numerical Assessment Criteria – ALMANAC (KINIRY et al., 1992), CROPGRO-Perennial-Forage model from Decision

Support System for Agrotechnology Transfer – DSSAT (JONES et al., 2003), Agricultural Production Systems Simulator – APSIM (MCCOWN et al., 1996), Environmental Policy Integrated Climate – EPIC (WILLIAMS et al. 1989), and the Jouven model (Jouven et al., 2006) are just a few examples of them. However, it is important to mention that most of the existing vegetation model was developed for farming purposes and, despite their variety, there are few references to vegetation growth models designed for urban areas, where vegetation growth is influenced by different situations and undergoes regular mowing processes.

Therefore, the main purpose of this work is to implement a grass growth model adapted to urban area conditions adopting the concepts of models already developed. Thus, this paper identifies the key variables to vegetation growth models in urban areas and advance on its implementation. It also presents a case study using bahiagrass (*Paspalum notatum* Flügge) as input for the model. Furthermore, once the model is effectively implemented, all UGS (composed mainly by grasses) of an area of interest will be integrated with the support of georeferenced data, producing a simulation for the whole urban area. Thus, the model may be considered a promising tool for management of UGS, specifically in lawns, public parks squares, roadsides and around waterways.

2.3. MATERIAL AND METHODS

2.3.1. Model structure

Fig. 1 illustrates the structure of the grass model, which incorporates components mainly from three models: EPIC (WILLIAMS et al. 1989), ALMANAC (KINIRY et al., 1992), and the J model (JOUVEN et al., 2006a). The model was implemented in Python 3.7, which is a user-friendly open-source programming language. Phyton provides tools suited to many applications and integrates well with geographical information systems (GIS), such as QGIS and ArcGIS.
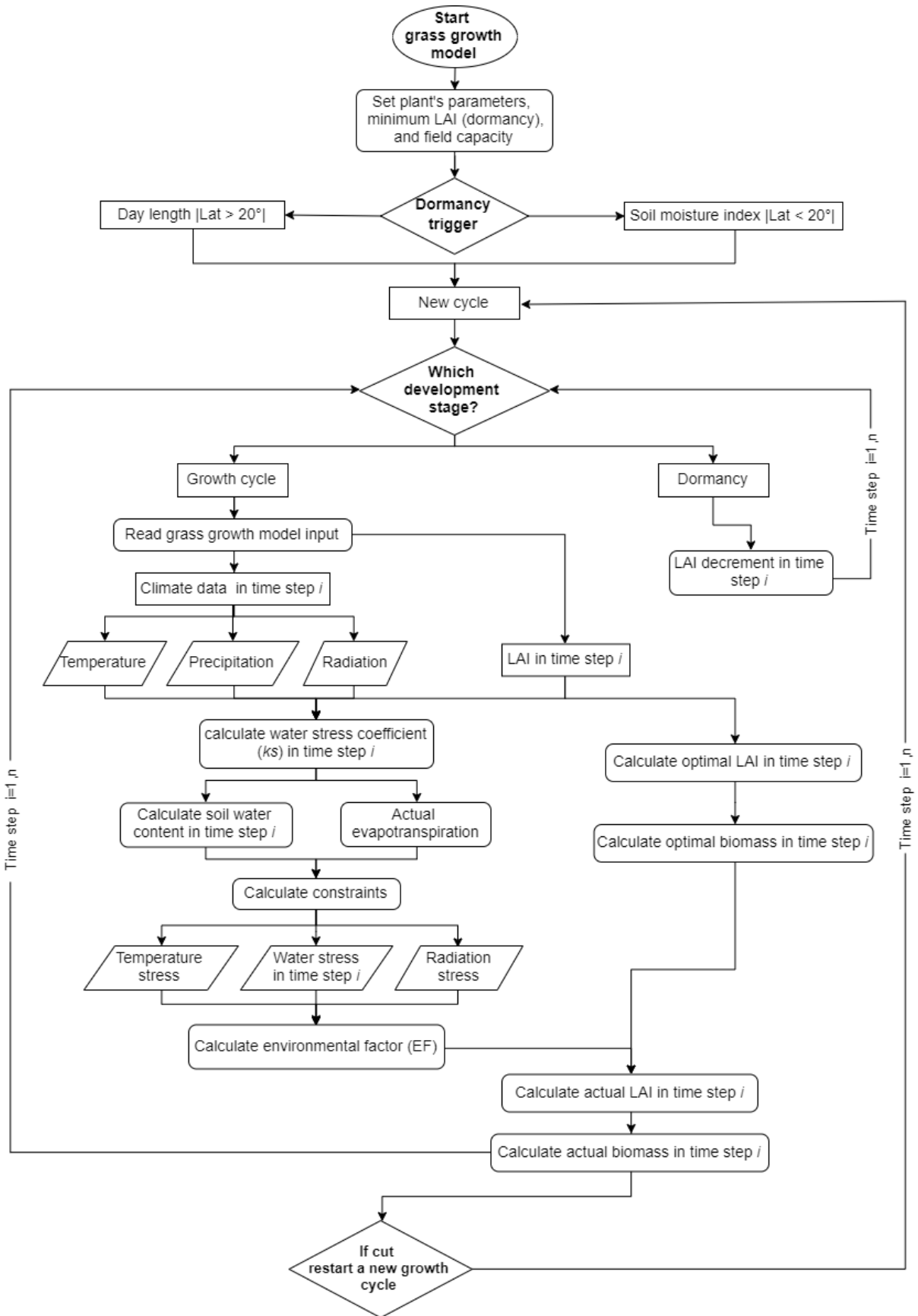
Figure 1: A framework for the adapted vegetation growth model. Source: author.

Regarding the plant growth, the phenological development is hereby simulated based on daily cumulative heat units, the potential biomass production is calculated using Monteith's approach (MONTEITH, 1977), and growth constraints are controlled by stress factors. Water, temperature, and radiation stress are considered the only environmental growth limitations. The model neither estimates the nutrient uptake by plants nor its potential stress since there are no records of the nutrient content in urban area soils.

Modeling of vegetation growth dynamic is driven as a function of leaf area development, the light interception and conversion of intercepted light into biomass adopting a plant species-specific radiation-use efficiency. Leaf area development is guided by the maximum leaf area index (LAI), the accumulated heat unit on the day and two shape coefficients of the plant, which must be provided by the user of the model. The model simulates two complementary scenarios using daily time steps. The first one runs all variables under optimal conditions, and afterward, the second one generates the actual values (real situation) as a function of the potential plant growth and the maximum value of the stress factors (constraints).

To terminate growing seasons and to repeat the annual growth cycles, the model provides the components dormancy for the grass species. The model is also able to reset the growth cycles after regular mowing processes. Daily precipitation, daily temperature (average, minimum and maximum) and daily solar radiation are the minimum weather data required to run the model. Two conditions may be used to trigger the dormant period (depending on the latitude of the study area), daylength or soil moisture index. The model is better described in the next section.

2.3.2. Grass growth model

Grass growth modeling depends on several factors (management, vegetation, soil and weather conditions) and hence a challenging task. This section presents the components which regulate the growth and dormant cycles adopted in the implemented model.

2.3.2.1. Heat unit

Temperature plays one of the most important roles in the control and development of plant growth, acting as a limiting factor. The heat unit (HU) approach assumes a direct relation between plant growth and temperature, which allows to quantify and link plants heat unit requirement to the time of planting and maturity. Each plant has its own temperature requirements. To experience any growth, plant's base temperature must be exceeded. Above the minimum temperature, the growth rate increases as a function of temperature until it reaches the range of optimum temperature. Once the optimum temperature range is exceeded, the growth rate starts to decrease as the temperature goes up until it reaches the maximum tolerated temperature is reached, at when growth ends. There is no growth below or at the base temperature and at or above the maximum temperature (NEITSCH et al., 2011; WILLIAMS et al., 1989).

The HU approach has been used since about 1730 (WANG, 1960; MEDERSKI, MILLER, WEAVER, 1973) and the cumulative effect of daily air temperature over the growing season has proven to be a reliable predictor of the plant physiological growth as well as a descriptor of maturity (GILMORE, ROGERS, 1958). HU measures the amount of heat energy that is accumulated by a plant on a given day (PENG, KRIEG, HICKS, 1989) and it is obtained by calculating the daily maximum and minimum air temperature and subtracting the base temperature of the plant (NEITSCH et al., 2011; WILLIAMS et al., 1989). The plant's base, optimum and maximum temperature may vary among species.

The formulation to calculate the HU is presented below (ARNOLD et al., 1998; NEITSCH et al., 2011):

when $T_{av,i} > T_{base}$ (2.1)

$$HU_i = \frac{T_{mx,i} + T_{mn,i}}{2} - T_{base}$$

and when $T_{av,i} \leq T_{base}$

$$HU_i = 0$$

where HU_i is the number of accumulated heat unit on day i (heat units), $T_{mx,i}$ and $T_{mn,i}$ are respectively the maximum and minimum air temperatures (°C) for day i, and T_{base} is the base temperature for growth (°C). No growth occurs for average temperatures at or below T_{base}.

A heat unit index (HUI), which varies from 0 at planting or the start of the growing season (for perennial grasses) to 1 at physiological maturity, is calculated by summing all daily HU accumulated during a growing season and dividing the resulting value by the number of the total heat units required for maturity (NEITSCH et al., 2011; ESPARZA et al., 2007):

$$HUI_{i,k} = \sum_{k=1}^{i} HU_k \bigg/ PHU \tag{2.2}$$

where $HUI_{i,k}$ is the heat unit index for day k and PHU is the number of the total heat units required for vegetation maturity. The value of PHU must be given by the user, considering that each plant has its own total heat unit requirement for maturity. PHU is also referred as potential heat units. For trees and perennials, however, PHU refers to the number of the total heat units required (or the number of days) from budding to leaf dormancy.

2.3.2.2. Dormancy

The model simulates the plant dormant period, at which there is no growth. At the beginning of the period, a fraction of the biomass (or total biomass depending on the species) is converted into residue and the leaf area of the plant starts to decline (NEITSCH et al., 2011). Dormancy is modeled assuming that there is a continuous decrease in rate of accumulation (JOHNSON, AMEZIANE, THORNLEY, 1983). The model presents two different approaches to trigger these periods:

i)   based on daylength (daylight hours) and latitude, which is more suitable for temperate regions (latitude ≥ 20°). The dormant period starts when the daylength approaches its annual minimum threshold and ends once the

daylength exceeds this minimum daylength in Spring (NEITSCH et al., 2011).

ii) from a soil moisture index (SMI), suitable for vegetation growth in monsoon-driven or tropical climates (latitudes between 20º S and 20º N), where vegetation growth dynamics are mainly controlled by the water availability in the soil profile rather than temperature (BORCHERT, 1994; JOLLY, RUNNING, 2004; ZHANG et al., 2005). Thus, the dormant period is triggered when the SMI reaches a predefined minimum value during the drought season, and it ends once the SMI exceeds this value. It is worthy to mention that it is harder to distinguish between dry and wet season within the tropics as the study area gets closer to the equator, once there is no pronounced season in this area (MCGREGOR, NIEUWOLT, 1998).

In both cases, the thresholds are defined by the user. The daylength is calculated as suggested by Allen et al. (1998):

$$N = \frac{24}{\pi} \times \omega_s \tag{2.3}$$

with

$$\omega_s = arccos[-tan(\varphi) \times tan(\delta)] \tag{2.4}$$

$$\varphi = \frac{\pi}{180} \times [Latitute\ in\ decimal\ degrees] \tag{2.5}$$

$$\delta = 0.409 \times sin\left(\frac{2\pi \times J}{365} - 1.39\right) \tag{2.6}$$

where N is the daylength (the number of daylight hours), ω_s is the sunset hour angle in radians and π is a mathematical constant, Φ is latitude in radians, δ is the solar declination, and J is day of the year.

The soil moisture index (SMI) is derived from the ratio between monthly precipitation and evapotranspiration (ALEMAYEHU et al., 2017):

$$SMI = \frac{P}{ET_o} \tag{2.7}$$

where P and ET_o are precipitation and the reference evapotranspiration for the crop (mm), respectively. For more representative estimates, P and ET_o may be obtained from long-term climate data.

2.3.2.3. Evapotranspiration and soil water content

Potential transpiration is a function of the reference evapotranspiration (described below) adjusted for the evaporation of the amount of the water held in the canopy and LAI. In this work, LAI corresponds to half the total developed area of green leaves per unit of horizontal ground area (WATSON, 1947; CHEN, BLACK, 1992). The value for the potential transpiration is the portion of the occurring maximum transpiration on a given day having no water constraint, and as a function of plant's LAI. Potential transpiration is computed as follows (NEITSCH et al., 2011):

when $0 \leq LAI \leq 3.0$ $\hspace{4cm}$ (2.8)

$$Et_P = \frac{E_o' \times LAI}{3.0}$$

when $LAI > 3.0$

$$Et_P = E_o' \tag{2.9}$$

where Et_P is the potential (maximum) transpiration (mm), E_o' is the reference evapotranspiration adjusted for the evaporation of water held in the plant canopy (mm), i.e. remaining evaporative water demand (mm), and LAI is the leaf area index.

The remaining evaporative water demand is then calculated from any rainfall intercepted by the plant canopy and reference evapotranspiration (NEITSCH et al., 2011) in such a way that:

when $ET_o > E_{can}$

$$E'_o = ET_o - E_{can}$$

$$(2.10)$$

when $ET_o \leq E_{can}$

$$E'_o = 0$$

where E_{can} is the amount of evaporation from water held in the canopy (mm) on a given day.

The reference evapotranspiration (ET$_o$) can be estimated from several methods, being the FAO Penman-Monteith method considered as the standard for computation of E_{to} from meteorological data (ALLEN et al., 1998). The Penman-Monteith method requires inputs such as solar radiation, air temperature, relative humidity, and wind speed. However, due to the possible absence of some of the mentioned variables and to avoid simulation of the missing required inputs, this model presents an alternative to calculate the reference evapotranspiration, the Hargreaves method (HARGREAVES, SAMANI, 1985). This alternative requires only solar radiation and air temperature, and it provides satisfactory results. It may be estimated as follows:

$$\text{ET}_o = \frac{[0.0023 \times R_a \times (T_{max} - T_{min})^{0.5} \times (T_{av} + 17.8)]}{\lambda} \qquad (2.11)$$

where R_a is the extraterrestrial solar radiation (MJ m^{-2}d^{-1}). T_{max}, T_{min} and T_{av} are respectively the maximum, minimum and mean air temperature (℃). λ is the latent heat of vaporization (MJ kg^{-1}).

The water held in the canopy is also expected to evaporate and the amount of this evaporation is calculated as follows (NEITSCH et al., 2011):

when $E_{to} > can_{storage}$ $\qquad\qquad\qquad\qquad\qquad\qquad\qquad\qquad$ (2.12)

$$E_{can} = can_{storage}$$

when $E_{to} \leq can_{storage}$ $\qquad\qquad\qquad\qquad\qquad\qquad\qquad\qquad$ (2.13)

$$E_{can} = E_{to}$$

where $can_{storage}$ is the actual amount of water stored in the canopy (mm) on a given day.

However, the described methods will depend on the amount of water that is effectively stored in the canopy on a given day, which is basically a function of the potential amount of water that can be trapped in the canopy and precipitation, in such a way that (NEITSCH et al., 2011):

when $P > can_P$ (2.14)

$$can_{storage} = can_P$$

when $P \leq can_P$ (2.15)

$$can_{storage} = P$$

where P is precipitation (mm), and $can_{storage}$ is the actual amount of water stored in the canopy (mm) on a given day.

On the other hand, the potential amount of water that can be held in the canopy on a given day depends on the maximum amount of water that can be trapped in the plant canopy when the canopy is fully developed (which varies among species), the maximum LAI and the LAI on day i (NEITSCH et al., 2011):

$$can_P = can_{mx} \times \frac{LAI_i}{LAI_{mx}}$$ (2.16)

where can_{mx} is the maximum amount of water (mm) that can be trapped in the canopy when the canopy is fully developed, LAI_{mx} is the maximum leaf area index for the plant.

After determining the conditions for the water on the canopy, actual transpiration may be calculated from potential transpiration (Eq. 2.8) and the water stress coefficient (K_s), as proposed below. K_s is a function of field capacity, depletion point, and permanent wilting point (Fig. 2). Allen et al. (1998) proposed a K_s with a linear decrease but in this work, it was assumed that a sigmoidal decay may be a more realistic approach. K_s is equal 1 when there is no water stress and is less than 1 (and greater or equal to zero):

when $K_s = 1$ (2.17)

$$Et_{act} = Et_P$$

when $0 \leq K_s < 1$ (2.18)

$$Et_{act} = Et_P \times K_s$$

with (2.19)

$$K_s = \frac{\tanh\left(\dfrac{\beta \times \left(SW - \dfrac{(DP + PWP)}{2}\right)}{DP}\right)}{2} + 0.5$$

where Et_{act} is actual transpiration (mm), K_s is the water stress coefficient, β is a shape coefficient (which varies with the class of the soil), FC is field capacity (mm), SW is soil water (mm), DP is depletion point (mm), and PWP is permanent wilting point (mm).
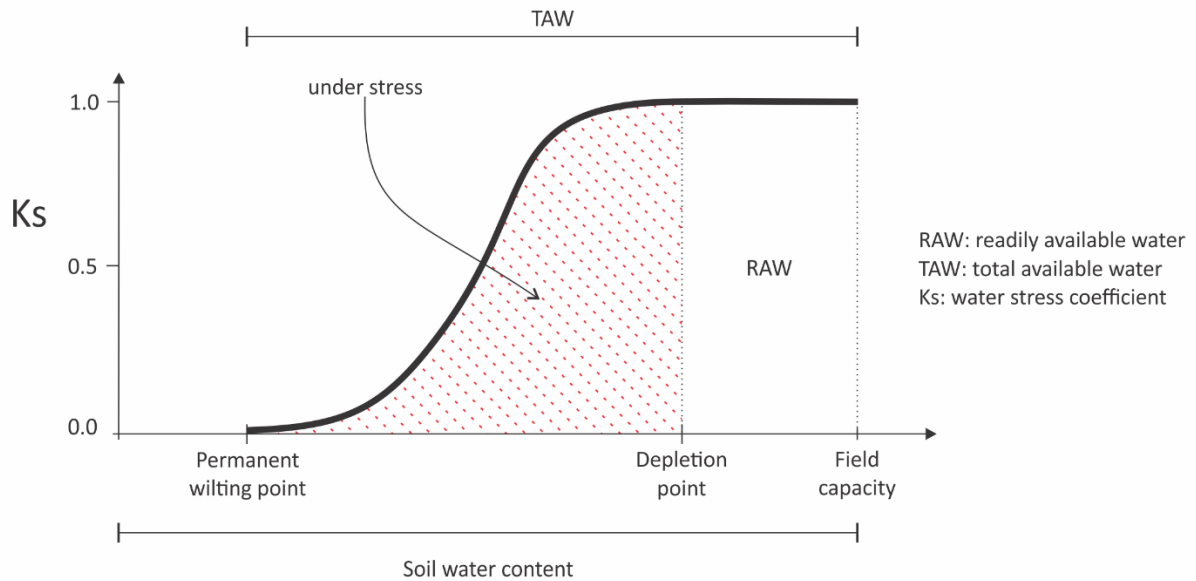
Figure 2: Proposed relation between water stress coefficient (K_s) and soil moisture. Source: author.

The soil water content may be calculated from a general equation of precipitation and two parameters, the retention water capacity of the soil (also known as field capacity) and terrain index (T_{idx}), which is here labeled as an estimate of the base flow. T_{idx} is obtained from a simplified exponential decay equation derived from HAND (Height Above the Nearest Drainage) method, which in turn, is a quantitative algorithm that normalizes the topography in respect to the drainage network on Digital Elevation Models (DEM) data (RENNÓ et al., 2008;

NOBRE et al., 2011). In summary, HAND uses a DEM to compute the vertical distance (height) of each grid cell in relation to the nearest stream cell it drains to (for a detailed description of the algorithm see RENNÓ et al., 2008). The elevation model used to calculate HAND results from a Digital Surface Model (DSM) with 5m resolution available from EMPLASA (São Paulo, 2013). The model was corrected for depressions/sinks and for artifacts on the DSM (stream burning technique) using ArcHydro tools within ArcGIS 10.2.

The combined use of water stress coefficient (K_s) with terrain index (T_{idx}) seeks to encompass the local soil water dynamic (related to water uptake by plants) and the drainage network, improving the simulation.

$$w_{soil,i} = (P \times \omega) - can_{storage} + w_{soil,i-1} \qquad (2.20)$$

$$w_{soil,f} = \left(w_{soil,i} - Et_{act}\right) \times T_{idx} \qquad (2.21)$$

with

$$T_{idx} = \frac{HAND_{log} - \min\left(HAND_{log}\right)}{\max\left(HAND_{log}\right) - \min\left(HAND_{log}\right)} \qquad (2.22)$$

where $w_{soil,i}$ is the amount of available water in the soil at the beginning of a given day (mm), ω is the field capacity for the site (when it is unknown, the models estimates this value from runoff curve number method (CN) and LAI), $w_{soil,i-1}$ is the soil water content on the previous day (mm), $w_{soil,f}$ is the amount of available water in the soil at the end of a given day (mm), and T_{idx} is terrain index, an normalized estimation of the subsurface runoff rate; and $HAND_{log}$ is the value obtained with HAND method adjusted to a logarithmic scale.

Urban areas are expected to present a different drainage network structure and water flow compared to natural watersheds, especially considering the removal of vegetation and replacement of pervious areas with impervious surfaces. However, in this study, it was assumed that UGS present a well-developed soil and, therefore, are not affected by these possible differences.

2.3.2.4. Potential vegetation growth

As previously mentioned, vegetation growth is obtained for two conditions: potential growth and actual growth. The potential vegetation growth modeling is obtained by the simulation of the potential increase in plant biomass under ideal growing conditions. The potential increase in biomass for a given day is basically a function of intercepted light and the plant's efficiency in converting light into biomass, assuming a specific plant species radiation-use efficiency – RUE (NEITSCH et al., 2011).

The interception of solar radiation by the leaf area of the plant is estimated using Beer's law (MONSI, SAEKI, 1953):

$$H_{phosy,i} = 0.5 \times H_{day,i} \times \left(1 - \exp^{(-k_l \times LAI_i)}\right) \qquad (2.23)$$

where $H_{phosy,i}$ is the intercepted photosynthetic active radiation (MJ m^{-2}) on day i, $H_{day,i}$ is the total incident solar radiation (MJ m^{-2}) on day i, k_l is the light extinction coefficient, LAI is the leaf area index on day i. $0.5 \times H_{day,i}$ is also kwon as the incident Photosynthetically Active Radiation – PAR (MJ m^{-2}).

The daily potential vegetation growth (kg ha^{-1}) is estimated from the relation between intercepted active radiation and radiation-use efficiency (MONTEITH, 1977):

$$PG_i = RUE \times H_{phosy,i} \qquad (2.24)$$

where PG is daily potential growth (kg ha^{-1}) on day i, also referred to as the daily potential increase in biomass, and RUE is the vegetation radiation-use efficiency (kg ha$^{-1} \cdot$ (MJ/m^2)$^{-1}$ or 10^{-1}g/MJ).

During the initial stage of growth, the optimal leaf area development is controlled by the fraction of the maximum LAI of the plant and two shape coefficients, which vary among species. Once the maximum leaf area index is reached, the LAI will remain constant until the onset of the dormant period, after which it starts to decline. The optimal leaf area development is calculated as follows (NEITSCH et al., 2011):

$$\text{fr}_{\text{LAImx},i} = \frac{\text{HUI}_i}{\text{HUI}_i + \exp^{(l_1 - l_2 \times \text{HUI}_i)}} \tag{2.25}$$

$$l_1 = \ln\left[\frac{\text{HUI}_1}{\text{fr}_{\text{LAI},1}} - \text{HUI}_1\right] + l_2 \times \text{HUI}_1 \tag{2.26}$$

$$l_2 = \frac{\left(\ln\left[\frac{\text{HUI}_1}{\text{fr}_{\text{LAI},1}} - \text{HUI}_1\right] - \ln\left[\frac{\text{HUI}_2}{\text{fr}_{\text{LAI},2}} - \text{HUI}_2\right]\right)}{\text{HUI}_2 - \text{HUI}_1} \tag{2.27}$$

where, $\text{fr}_{\text{LAImx},i}$ is the fraction of the plant's maximum LAI on day i, l_1 is the first shape coefficient for optimal leaf area development curve and l_2 is the second shape coefficient for optimal leaf area development curve. HUI_1 is the fraction of growing season (i.e. fraction of total potential heat units) corresponding to the 1$^{\text{st}}$ (first) point on the optimal leaf area development curve, $\text{fr}_{\text{LAI},1}$ is the fraction of the maximum plant leaf area index (i.e. fraction of LAI_{mx}) corresponding to the 1$^{\text{st}}$ (first) point on the optimal leaf area development curve, HUI_2 is the fraction of growing season corresponding to the 2$^{\text{nd}}$ (second) point on the optimal leaf area development curve and $\text{fr}_{\text{LAI},2}$ is the fraction of the maximum plant leaf area corresponding to the 2$^{\text{nd}}$ (second) point on the optimal leaf area development curve.

For annual and perennial species, the potential increase added in the leaf area on day i is estimated as suggested by Neitsch et al. (2011):

$$\Delta\text{LAI}_i = \left(\text{fr}_{\text{LAImx},i} - \text{fr}_{\text{LAImx},i-1}\right) \times \text{LAI}_{\text{mx}} \times \left(1 - \exp^{(5 \times (\text{LAI}_{i-1} - \text{LAI}_{\text{mx}}))}\right) \tag{2.28}$$

where, ΔLAI_i is the potential LAI increment on day i, $\text{fr}_{\text{LAImx},i}$ and $\text{fr}_{\text{LAImx},i-1}$ are the fractions of the plant's maximum leaf area index on days i and $i-1$, respectively. LAI_{i-1} is LAI on the previous day $i-1$ and LAI_{mx} is the maximum leaf area index (it is provided by the user of the model).

Based on Eq. 2.28, the potential total LAI is computed as function of potential LAI of the previous day and the LAI increment (NEITSCH et al., 2011):

$$LAI_{P,i} = \Delta LAI_i + LAI_{i-1}$$
(2.29)

where $LAI_{P,i}$ is the potential total LAI on day i, ΔLAI_i is the potential LAI increment on day i and LAI_{i-1} is the LAI of the day before.

2.3.2.5. Environmental constraints on growth

Real plant growth may vary from potential plant growth (Eq. 2.24) due to the constraints caused by environmental stress factors (SCHAPENDONK et al., 1998; NEITSCH et al., 2011). The present model evaluates daily stresses caused by temperature, available water in the soil, and solar radiation. It is worth mentioning that since there are no records for the nutrient content in urban area soils, the model does not estimate the nutrient uptake by plants nor its potential stress. For each considered factor, the stress varies from 0.0 (under optimal conditions with the maximum growth rate) to 1.0 (no growth), which directly affect the plant development during the growing season. A better description of these factors is presented ahead.

Temperature stress (T_{str}) is used to evaluate the daily impact caused by air temperature variation in relation to the optimal temperature for the plant growth and development (ZAMAN, MORID, DELAVAR, 2016; NEITSCH et al., 2011). In summary, plants will not be subjected to temperature stress within the optimal temperature range (considering that some species present an optimal temperature range). However, the more the air temperature diverges from the plant's optimal temperature, the more the plant suffers from temperature stress (NEITSCH et al., 2011). No growth occurs when the mean daily temperature is at base temperature or below, and at or above the maximal acceptable temperature.

The range and equations used to determine temperature stress are (SCHAPENDONK et al., 1998):

when $T_{av,i} = T_{opt}$ (2.30)

$$T_{str,i} = 0$$

when $T_{min} < T_{av,i} < T_{opt}$ (2.31)

$$T_{str,i} = 1 - \frac{T_{\text{av},i} - T_{min}}{T_{opt} - T_{min}}$$

when $T_{opt} < T_{\text{av},i} < T_{max}$ (2.32)

$$T_{str,i} = 1 - \frac{T_{\text{av},i} - T_{max}}{T_{opt} - T_{max}}$$

when ($T_{\text{av},i} \leq T_{min}$ and $T_{\text{av},i} \geq T_{max}$) (2.33)

$$T_{str,i} = 1$$

where T_{str} is the temperature stress on day i, $T_{\text{av},i}$ is the mean air temperature on day i (°C), and T_{min}, T_{opt} and T_{max} are the minimal, optimal and maximum temperatures (°C) for growth, respectively.

Soil water stress (W_{str}) is based on the evapotranspiration conditions. For this work, W_{str} is a function of the water stress coefficient (Eq. 19), being equal to 0.0 when soil water content is optimal and increases up to 1.0 as soil water approaches the permanent wilting point. It is obtained as follows:

when DP < SW ≤ FC (2.34)

$$W_{str,i} = 0$$

when SW < DP (2.35)

$$W_{str,i} = \max (1 - K_s)$$

where $W_{str,i}$ is the soil water stress on day i.

Solar radiation stress (Rad_{str}) is a function of photosynthetically active radiation – PAR (MJ m^{-2}). Based on Schapendonk et al. (1998) and Jouven, Carrère and Baumont, (2006), the plant growth starts to be constrained when PAR is higher than 5 MJ m^{-2}, i.e. the RUE decreases for PAR above 5 MJ m^{-2}, and no growth is expected when PAR is at or higher than 28 MJ m^{-2} (Fig. 3). It is computed as follows:

when $PAR < 5$ (2.36)

$$Rad_{str,i} = 0$$

when $PAR > 5$ (2.37)

$$Rad_{str,i} = 0.044 \times (PAR - 5)$$

if $Rad_{str,i} = 0.044 \times (PAR - 5) > 1$ (2.38)

$$Rad_{str,i} = 1$$

where PAR is photosynthetically active radiation on a given day (MJ m^{-2}). Above a specific threshold, the higher the PAR, the higher the solar radiation stress.
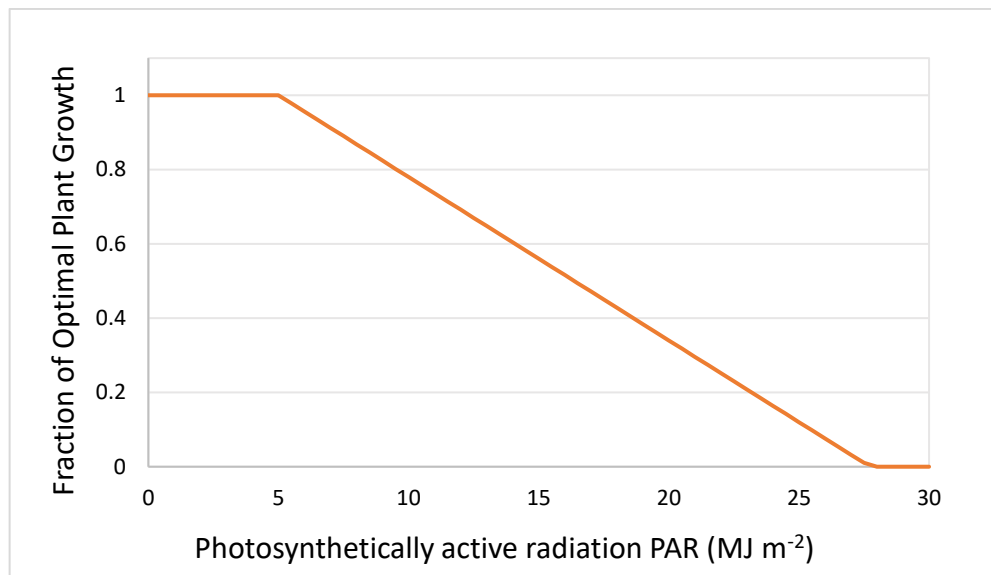
Figure 3: Upper and lower thresholds of the impact of photosynthetically active radiation (PAR) on the fraction of the optimal plant growth. Source: SCHAPENDONK et al., 1998.

The environmental factor (EF), previously discussed and referred as stress factor, quantifies the environmental limitation undergone by the potential growth. EF is controlled by the greatest value of the three constraint parameters showed previously (temperature, water availability and solar radiation), and higher stress conditions implicate on lower EF values (NEITSCH et al., 2011):

$$EF_i = 1 - \max{(T_{str,i}, W_{str,i}, Rad_{str,i})}$$ (2.39)

where EF represents the growth limitation by environmental factors on a given day. T_{str}, W_{str} and Rad_{str} are the temperature, water and solar radiation stress, respectively.

2.3.2.6. Actual vegetation growth

Based on the environmental stress factors, the actual plant growth may be computed as the product of the daily potential growth obtained in optimum conditions and the environmental factor at the same day (NEITSCH et al., 2011; SCHAPENDONK et al., 1998):

$$RG_i = PG_i \times EF_i \qquad (2.40)$$

where RG_i is the real growth or the actual biomass accumulated on day i ($kg\ ha^{-1}$) and EF_i represents the environmental growth constraints given day i.

Subsequently, the biomass ($kg\ ha^{-1}$) on a given day is calculated based on the actual biomass (RG) and the biomass at the end of the previous day ($kg\ ha^{-1}$) (NEITSCH et al., 2011; HAN et al., 2015):

$$bio_i = RG_i + bio_{i-1} \qquad (2.41)$$

where bio_i is the biomass at the end of the day i ($kg\ ha^{-1}$) and bio_{i-1} is the biomass at the end of the previous day ($kg\ ha^{-1}$).

The potential leaf area added on a given day in Eq. 2.28 may be also adjusted as follows (NEITSCH et al., 2011):

$$\Delta LAI_{act,i} = \Delta LAI_i \times \sqrt{EF_i} \qquad (2.42)$$

where $LAI_{act,i}$ is the actual leaf area index added on day i.

Then, the total leaf area index for a given day is computed as follows (NEITSCH et al., 2011):

$$LAI_i = LAI_{i-1} + \Delta LAI_{act,i} \tag{2.43}$$

where LAI_i and LAI_{i-1} are the leaf area index on day i and leaf area index on day before, respectively.

2.3.2.7. LAI decrement

The mentioned conditions above refer to the growing period. Once the stage of dormancy is started, the LAI starts to decline, and for this model, the conditions for this period are being estimated as suggested by Strauch and Volk (2013):

$$LAI_i = \left(\frac{LAI_{mx,d} - LAI_{min,d}}{1 + \exp^{(t)}} \right) + LAI_{min,d} \tag{2.44}$$

with $\tag{2.45}$

$$t = (-12) \times (r - 0.5)$$

$$r = \frac{1 - HUI}{1 - dlai} \tag{2.46}$$

where the term used as the exponent is a function of time (t), and $LAI_{mx,d}$ and $LAI_{min,d}$ are the maximum and minimum leaf area index expected during dormancy, respectively. $dlai$ is a user-defined fraction of PHU (model parameter DLAI).

It is important to mention that the daily values of LAI presented in this work do not apply for trees. In this case, the leaf area development is controlled by the age of the trees, and LAI_{max} depends on the number of years for the tree species to reach full development (NEITSCH et al., 2011). All parameters of the vegetation model are listed in Table 1.

Table 1: Parameters of the vegetation model adapted for urban areas.

Parameter	Units	Description
RUE	kg ha^{-1}·(MJ/m^{-2})$^{-1}$ or 10^{-1}g/MJ	Vegetation radiation-use efficiency
LAI_{mx}	m^{-2} /m^{-2}	Maximum leaf area index for the plant
$LAI_{mx,d}$	m^{-2} /m^{-2}	Maximum LAI expected during dormancy
$LAI_{min,d}$	m^{-2} /m^{-2}	Minimum LAI expected during dormancy
$dlai$	-	User-defined fraction of PHU (model parameter DLAI)
l_1		First shape coefficient for optimal leaf area development curve
l_2	-	Second shape coefficient for optimal leaf area development curve
HUI_1	-	A fraction of growing season (i.e. fraction of total potential heat units) corresponding to the 1st (first) point on the optimal leaf area development curve
$fr_{LAI,1}$	-	A fraction of the maximum plant leaf area index (i.e. fraction of LAI_{mx}) corresponding to the 1st (first) point on the optimal leaf area development curve
HUI_2	-	A fraction of growing season corresponding to the 2nd (second) point on the optimal leaf area development curve
$fr_{LAI,2}$	-	A fraction of the maximum plant leaf area corresponding to the 2nd (second) point on the optimal leaf area development curve
T_{min}	°C	Plant's minimal (base) temperature for growth
T_{opt}	°C	Plant's optimal temperature for growth
T_{max}	°C	Plant's maximum temperature for growth
k_l	-	A light extinction coefficient
PHU	-	Potential heat unit required for maturity

2.3.2.8. Mowing processes

The model allows the user to set up mowing processes. For each mowing event, all output data is stored before the model returns to its initial configuration, which should have already been provided by the user (e.g. temperature requirements, minimum and maximum LAI, PHU, dormancy trigger, etc.). Then, a new growth cycle is started. A detailed illustration of the mowing process component in a study case is shown in section 3.

2.3.3. Study area

In the present work, a snip in the southwestern of the urban area of São Carlos city (21º30' – 22º30'S, and 47º30' – 48º30'W) was used. The city is situated in the center-east of São Paulo state, in the southeast region of Brazil (Fig. 4). There are 204 UGS (including public squares, lawns, and edges of waterways) within the sniped area, totalizing 1.28 km^2 (green polygons in Fig. 3). The altitude in the area ranges from 704 to 861 m above sea level. Climate, based on information for the city of São Carlos and following Köppen's system (1931), is classified as Cwa (tropical climate of altitude), and we separated it into i) wet summer, from October to April (seven months); ii) and dry winter, from June to August (three months). In this work, monthly average precipitation and temperature were generated using 27-year-data (1992 – 2018) from the Embrapa Pecuária Sudeste agrometeorological station (21°57'42" S and 47°50'28" W, altitude of 860 m, BRAZIL – EMBRAPA, 2019) located approximately 12 km from the area of interest. From the data, May and September were classified as transitions months. Mean annual rainfall and temperature (period 1992–2018) lie at 1,415.4 mm and 21.4 ºC, respectively, as shown in Fig. 5.
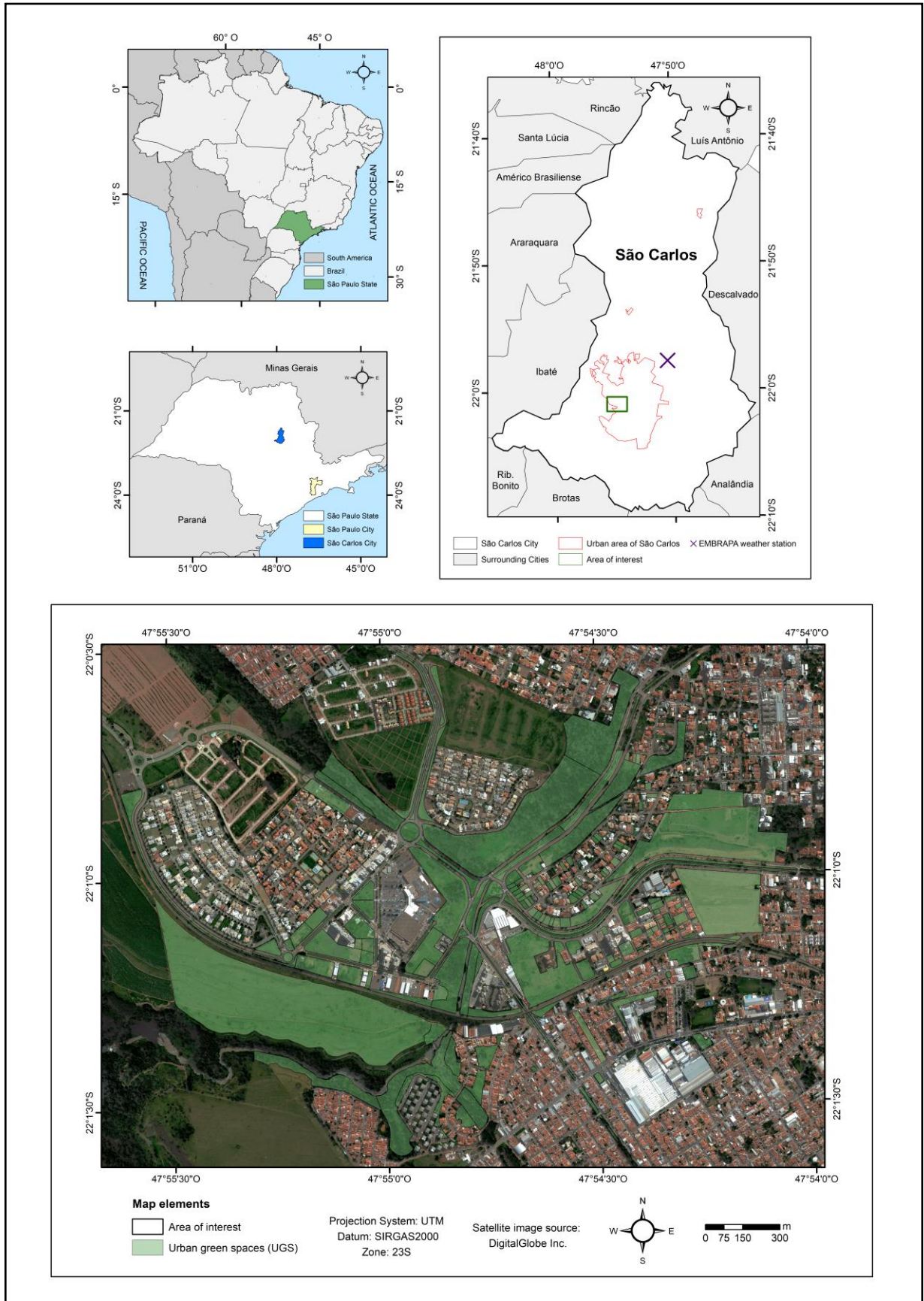
Figure 4: Location map for the area of interest, which is located in São Carlos, São Paulo, Brazil. There are 204 UGS (green polygons) within the sniped area, totalizing 1.28 km^2.
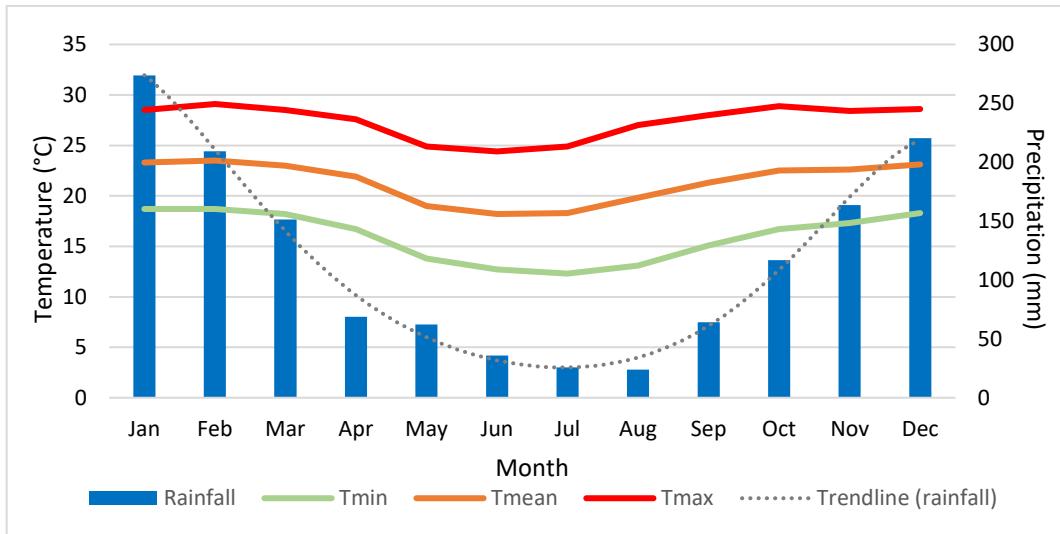
Figure 5: Annual variation of temperature and precipitation based on 27-year-data (1992–2018): São Carlos, São Paulo, Brazil.

2.3.4. Growth simulation

Considering that many variables of the model depend on values that are intrinsic to each vegetation species, we selected bahiagrass as input to run the model considering that i) this species is widely grown in urban public areas in Brazil, especially in lawns, and public parks and squares; ii) the UGS mapped in the area of interest are mostly composed by this species. It requires a base temperature of 12°C, an optimal temperature range from 32°C to 40°C, and a maximum temperature of 45°C for growth (RYMPH, 2004; KINIRY et al., 2007; PEDREIRA, BROWN, 2011). It was also assumed a light extinction coefficient of 1.1, a RUE of 1.6 (KINIRY et al., 2007) and a PHU of 3,300 for the study species. PHU is based on the annual mean of accumulated heat unit (i.e. higher than the base temperature) in the study area. Finally, independent simulations were performed in daily time steps for each one of the 204 UGS mapped in the area under consideration for the period from January to December of 2018.

2.4. RESULTS AND DISCUSSION

To effectively run the model, the user first needs to set up the plant's parameters, the minimum value for the dormant period, for the approach which will be used to start

dormancy and field capacity. (see Section 2.2.2). Hereafter, it is presented how the dormant period varies within the study area according to the two options available in the model.

For the daylength approach, the area under consideration had 284 for the growing season and 81 days for the dormant period in 2018, a year with 365 days (Table 2). Fig. 6 illustrates the daylength variation throughout the year. The shortest day in the study area has 10 hours and 39 min of daylight; thus, following this approach, when daylength reaches 11 hours (on May 10th), the model starts dormancy and it lasts until the daylength exceeds 11 hours again (July 29th).

Table 2: Number of days of growing season and dormant period according to daylength approach.

	GROWING SEASON			DORMANT PERIOD		
YEAR	DOY*	Period	Total (days)	DOY*	Period	Total (days)
2018	1-130	Jan 1st – May 9th	284	130-210	May 10th – Jul 29th	81
	211-365	Jul 30th – Dec 31st				

*DOY: day of year.
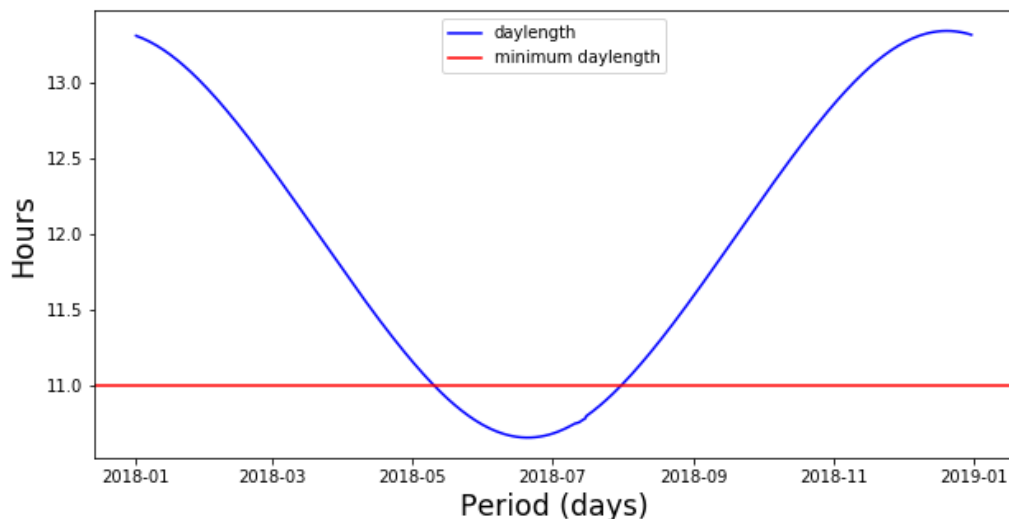
Figure 6: Daylength variation throughout the year in São Carlos, São Paulo, Brazil. The dormant period is considered while the daylight hours are less than 11 hours (red line).

Considering the SMI approach, which is more suitable for tropical areas (STRAUCH, VOLK, 2013), the limits for growing season and dormancy follow a long-term-annual-pattern, from which the wet season (October to April) and dry season (June to August) were identified. May and September were classified as transitions months. The dry season (from June to August) shows the lowest SMI values (less than 0.55), as expected (Fig. 7). Thereby, the dormant period has a 92-day-period while growing season, in the study area, has 274 days in leap years, and 273 days in normal years (Table 3).
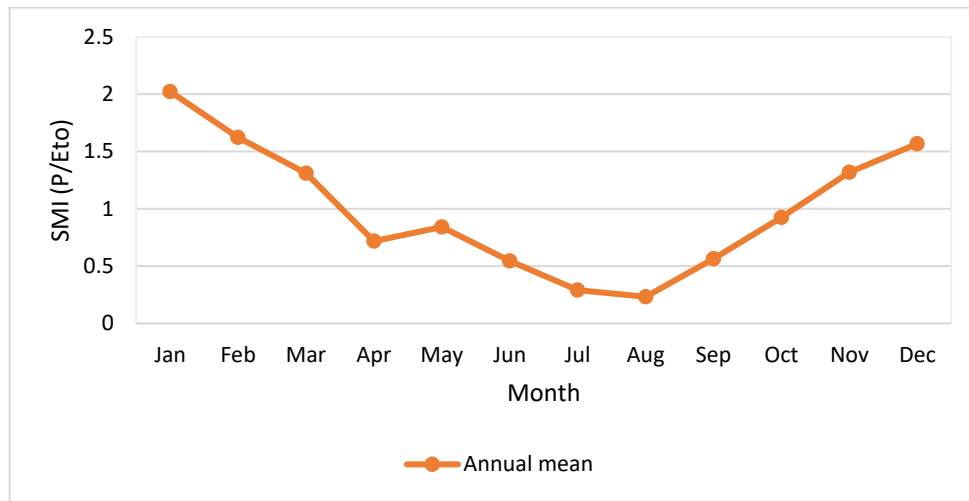
Figure 7*:* The average moisture index (SMI) derived from precipitation (P) and reference evapotranspiration (ET_o) based on observations from the annual mean (period 1992–2018) for São Carlos, SP, Brazil.

Table 3: Number of days of growing season and dormant period according to wet season approach.

	GROWING SEASON			**DORMANT PERIOD**		
YEAR	**DOY***	**Period**	**Total (days)**	**DOY***	**Period**	**Total (days)**
2018	1-151 244-365	Jan 1st – May 31st Sep 1st – Dec 31st	273	152-243	Jun 1st – Aug 31st	92

*DOY: day of year.

Fig. 8 illustrates the constraint of potential growth as temperature varies. Following the temperature requirements of bahiagrass, there is no growth below or at 12°C and at or above 45°C; and there is no temperature constraint for growth at or between 32°C and 40°C. Temperature constraint (0-1) is reduced when the daily air temperature nears 32°C and increases for temperature above 40°C. For temperatures above 45°C, the stress is maximum and there is no growth. Since the model was conceived to be used in different areas (spatially distributed) and for a wide range of species, this simple (partial) linear relationship between temperature and growth constraint seems reasonable. This approach is suggested when the plant response curve to temperature variations is unknown.
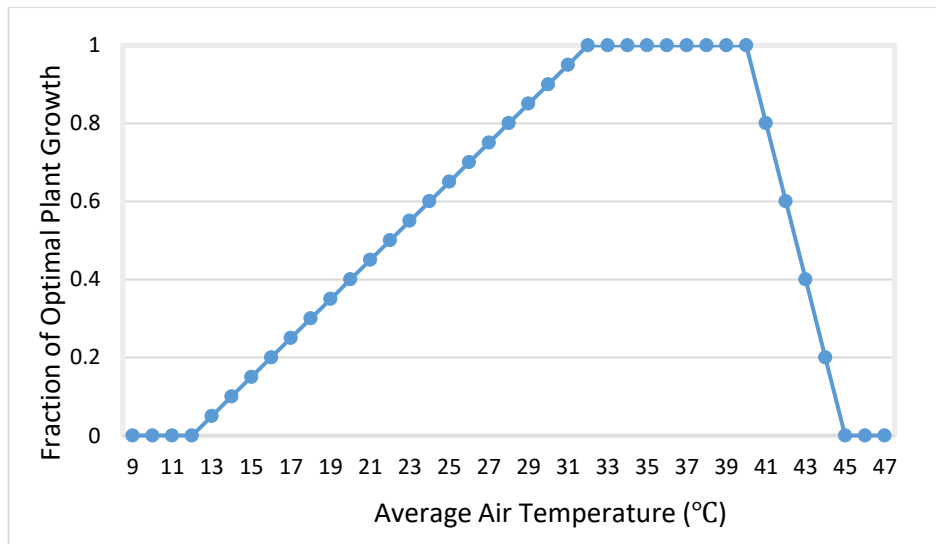
Figure 8: Thresholds of mean air temperature impact on the fraction of the optimal (potential) plant growth for bahiagrass. Source: RYMPH, 2004; KINIRY et al., 2007; PEDREIRA, BROWN, 2011.

After all input parameters are given and the dormancy trigger is set, the model starts running the simulations using daily time steps, first for optimal conditions (potential plant growth) and then for real conditions (under EF constraints). For this study, the model was executed for the period between January 1 of 2018 to December 31 of 2018, considering all 204 UGS as a single one. Fig. 9 presents the simulation of LAI change under optimal conditions with a maximum LAI of 3.2 and a minimum LAI of 0.5 (set at the beginning of the simulation). For this simulation, SMI was selected as the trigger for the dormant period, which starts on June 1, when LAI begins to decrease, and it lasts until August 31. Once dormancy is over, LAI starts to increase again. Under optimal conditions, LAI change is ruled by daily accumulation of heat

units only (Fig. 10). There was no accumulation of heat units during the dormant period (from June to August).
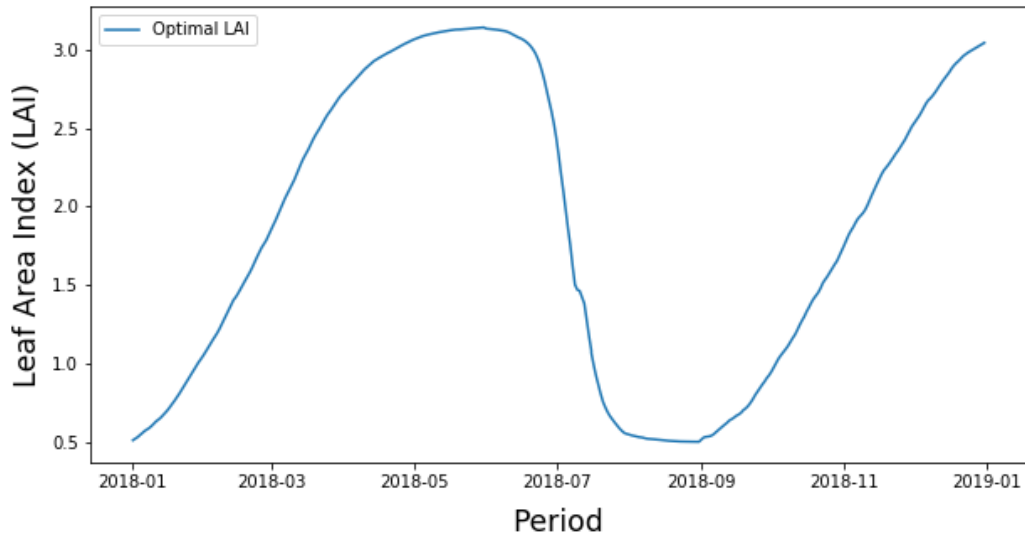
Figure 9: Daily Simulation of optimal LAI change for bahiagrass based on from SMI approach in São Carlos, São Paulo, Brazil for the year 2018. For initial LAI and minimum LAI during dormancy, a value of 0.5 was adopted.
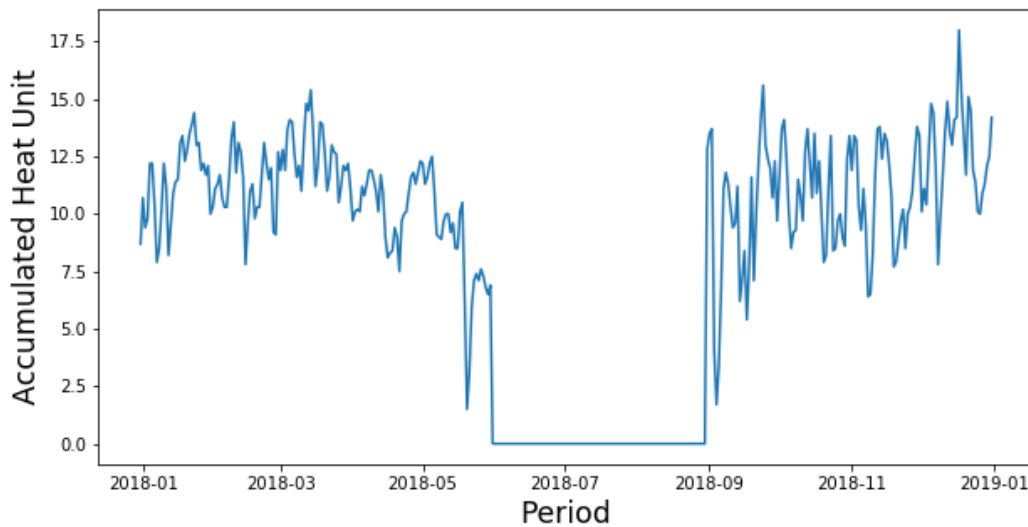
Figure 10: Daily accumulation of heat unit (2018) for bahiagrass with a base temperature of 12°C and a maximum temperature of 45°C in São Carlos, São Paulo, Brazil. There was no heat unit accumulation during the dormant period (from June to August).

As soon as daily potential plant growth is determined, the model starts simulating the actual plant growth. As stated earlier, it is calculated as a function of potential plant growth (Eq. 2.24) and EF (Eq. 2.39). Fig. 11 presents the variation of the three constraint parameters

in 2018, at which 0.0 means no stress and 1.0 means no plant growth. Water stress is not calculated during dormancy, thus from June to August, the water content in the soil is set to 0.0.
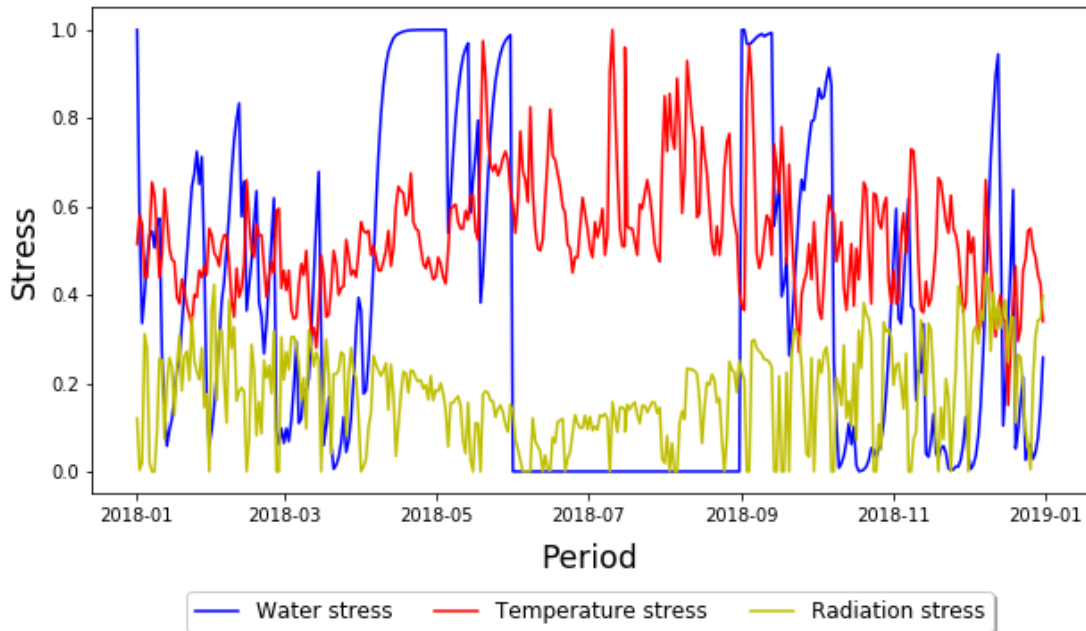
Figure 11: Daily plant's growth constraints (water, temperature and solar radiation stress) during the year 2018.

It is clear from Fig. 11 that water and temperature stress play the most constraints in plant growth for this study area. It is worth mentioning that water stress shows values of 1.0 (no plant growth) even in the wet season, which likely occurs due to the intense rain events followed by several days without any precipitation. Temperature stress presents its highest values in the period from the end of May to the beginning of September, which was expected since this period includes not only the winter season but its transitions. Lastly, radiation stress shows a low decrement from June to August, which is expected due to the reduction of the incident total solar radiation in this period.

Once the three constraint parameters are calculated, the EF of each day is determined. The model is implemented to select the greatest value of the three constraint parameters (water, temperature and solar radiation stress). Fig. 12 illustrates EF variation, which is inversely proportional to the greatest value of the constraint parameter, i.e. the higher

the constraint parameter values, the lower the EF values (Eq. 2.39). EF shows values 0.0 for the dry season (from July to August), once that this was set as the dormant period.
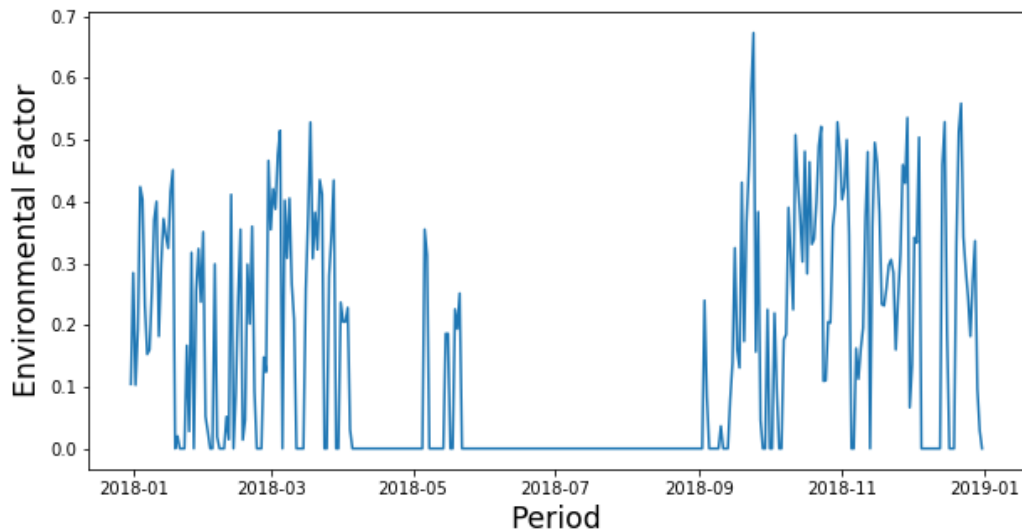
Figure 12: Daily variation of Environmental factor (EF) in 2018. EF was obtained from water, temperature and solar radiation stress.

After all steps above, real growth is calculated from the quantification of the fraction of potential growth achieved on each day by EF (Fig. 13). For the simulated period, it seems that there is a mean rate of biomass production for the period analyzed, with a slightly higher value for the period from September to December compared to the January to April interval. Furthermore, biomass production, also known as primary productivity, is presented in Fig. 13 and shows a substantial period without any growth in April, which is clearly an effect of the drought period for this month (as indicated by the water stress constraint in Fig. 11).
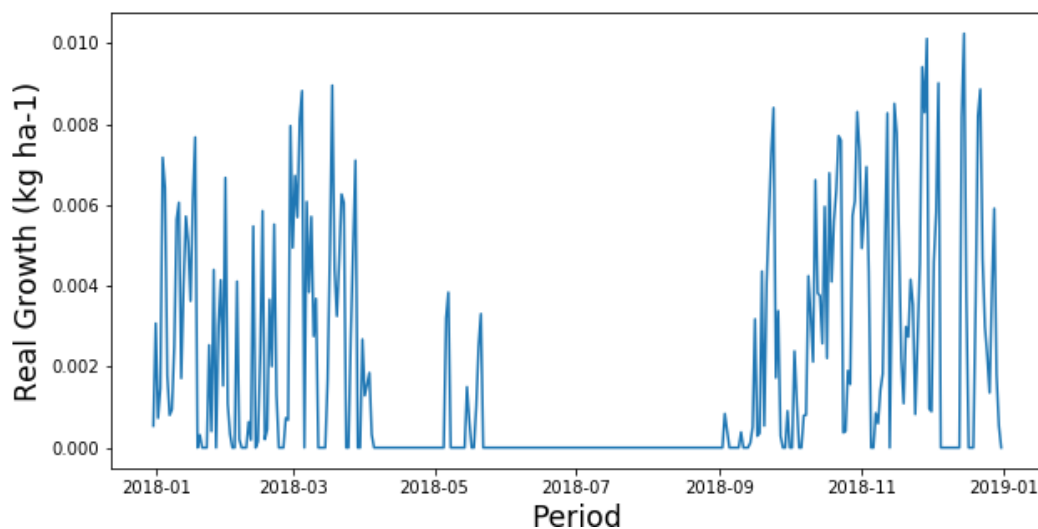
Figure 13: Daily real growth (kg ha^{-1}), also known as primary productivity, in 2018.

The outputs of optimal LAI (Eq. 2.29) and actual LAI (Eq. 2.43) for the period from January to December of 2018 are compared in Fig. 14. Actual LAI shows a maximum value of 2.15, while optimal LAI goes up to 3.2 (as stated before). It is apparent from Fig. 14 that actual LAI reaches its maximum value a little bit later than the optimal LAI, which is likely related to the delayed full development of the plant caused by the constraints of EF. It is important to highlight that actual LAI shows a very small growth right after dormancy is over, which is caused by high-water stress in this period (Fig. 11).
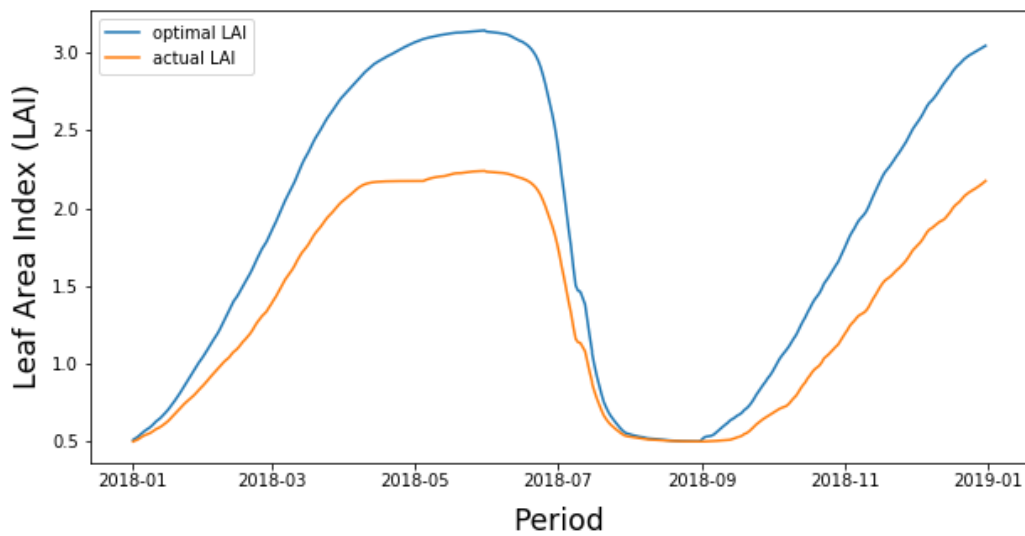
Figure 14: Comparison of actual and optimal LAI for the year 2018. An initial LAI of 0.5 was adopted.

Aiming to simulate the dynamics of the model with regular mowing processes (something that is expected under real conditions) and considering the location of each UGS, it is presented a simulation of the actual LAI chance (Eq. 2.43) during 2018 for all 204 UGS mapped in the study area (Fig. 15), now as independent areas. The initial and maximum LAI were set to 0.5 and 2.0, respectively, for this simulation. The main idea of this procedure was to spatialize the vegetation growth (using LAI as an indicator) considering the variations in soil water conditions according to the drainage network (subsurface runoff dynamics). Terrain index (see Eq. 2.21) was considered as an essential parameter, once it was assumed that there is no solar radiation and temperature variation within the UGS (i.e. all areas have the same temperature and solar radiation conditions).
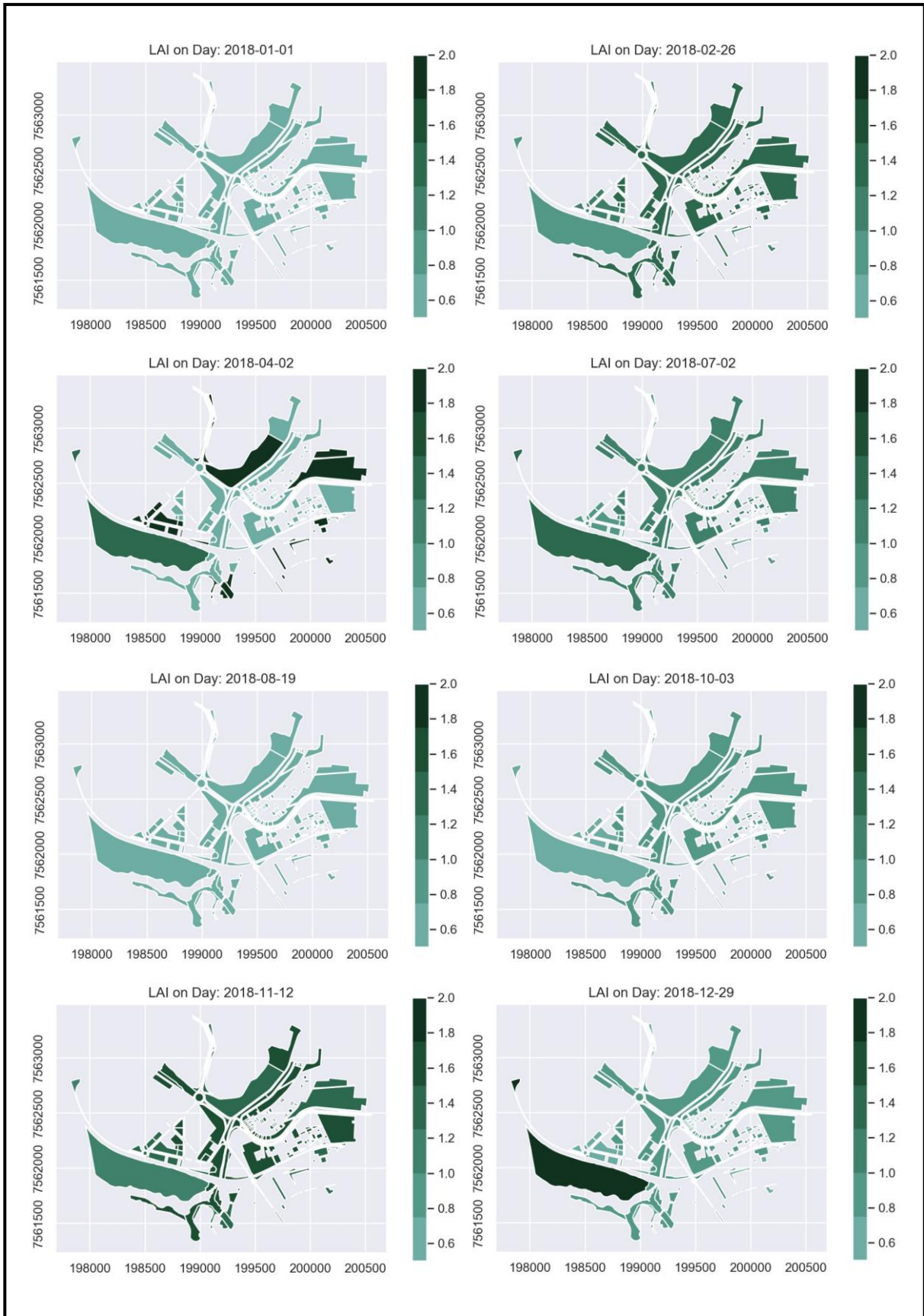
Figure 15: Actual LAI simulation for all UGS in the study area during the year 2018.

Eight stages of the LAI forecasting throughout the year 2018 for each area is displayed in Fig. 15, encompassing the four seasons. LAI values are displayed on a green scale so that the darker the green, the higher the LAI for the area. Soil moisture index was adopted in this simulation as the trigger for dormancy. To simulate plant growth with mowing regimes, it was considered that a new growth cycle would be started whenever the LAI of the area reached 2. Moreover, independently of the LAI before the dormant period, all areas reach a common minimum LAI (set by the user before the model is started) at the end of dormancy. It is also clear from the figure that areas which reach higher LAI first are closer to streams and/or at lower altitudes, hence not suffering from water stress as other elevated areas. However, in these areas, the mowing processes need to be cut more frequent. This approach not only provides the model a better representation of what happens in the environment but also helps the user to identify easily and faster the areas which need more attention regarding mowing management. Thus, the simulation presented in Fig. 15 represents a powerful tool for the management of UGS regarding mowing processes.

Despite the compelling results, there are still some limitations to be addressed that could improve the model. Future improvements would include shadow conditions, which are expected to make the model more reliable for green areas dominated by trees. Adjustments in the dormant period threshold are necessary as well to improve the response of the model for shorter (longer) dry (rain) seasons.

2.5. CONCLUSION

In this study, a grass growth model adapted to urban area conditions is proposed and implemented, which includes dormant period, a LAI approach based with a sigmoidal decrease toward a minimum value (defined by the user) during dormancy, the regular mowing process, and spatial capabilities (designed for GIS environment). Only above-ground growth is modeled. The model allows setting the dormant period based on two different approaches: daylength or the soil moisture index - SMI, which allows covering temperate and tropical areas. In addition, the implemented model incorporates the local soil water dynamic (related to water uptake by plant) based on the drainage network (subsurface runoff dynamics) to generate the soil water stress.

The idea of adopting a sigmoidal LAI decrease up to a minimum value during the dormant period, as suggested by Strauch and Volk (2013), seems to give reasonable results and might be considered more realistic to both perennial and annual plants compared to a linear decrease. Moreover, bearing a minimum LAI greater than zero allows the model to cover simulations for LAI of trees and other plants, which usually do not necessarily fall to zero during dormancy. It is also important to emphasize that the model does not consider senescent plants, which may be an interesting adjustment for the future.

Considering the spatial capabilities of the model, the dataset produced by the terrain index seems to be an interesting way to include groundwater level in the grass growth modeling and to spatialize the information of independent areas while the model runs, allowing integration with GIS. However, more studies in this field should be performed to better evaluate the results.

The model here described enables the simulation of the dynamics of LAI, biomass, evapotranspiration and soil water content at different scales. Furthermore, the model is able to simulate grass growth under mowing processes in urban environments. No previous studies on this subject were found in the literature. However, further adjustments should be accomplished to improve model performance, such as regulation of the dormant period threshold and the inclusion of shadow conditions. Lastly, this model may help government administrations with the optimization of cleaning/mowing processes of UGS, decreasing management expenses and ecosystem impacts, which consequently may increase the quality of life and well-being of citizens.

2.6. ACKNOWLEDGMENT

(USDA), James R. Kiniry (USDA), André Backes (UFU), Camilo Daleles Rennó (INPE), José Ricardo M. Pezzopane (EMBRAPA), and Paulo Guilherme Molin (UFSCar) for all scientific contributions.

2.7. REFERENCES

ALEMAYEHU, Tadesse; GRIENSVEN, Ann van; WOLDEGIORGIS, Befekadu Taddesse; BAUWENS, Willy. (2017). An improved SWAT vegetation growth module and its evaluation for four tropical ecosystems. Hydrology and Earth System Sciences, 21(9), 4449-4467. https://doi.org/10.5194/hess-21-4449-2017.

ALLEN, RICHARD G.; PEREIRA, Luis S.; RAES, Dirk; SMITH, Martin. (1998). Crop evapotranspiration-Guidelines for computing crop water requirements-FAO Irrigation and drainage paper 56. FAO, Rome, 300(9), D05109.

ARAUJO, Marla Alessandra; SOUZA, Jorge Luiz Moretti de; TSUKAHARA, Rodrigo Yoiti. (2011). Modelos agro-meteorológicos na estimativa da produtividade da cultura da soja na região de Ponta Grossa, Estado do Paraná. Acta Scientiarum. Agronomy, Maringá, v. 33, n. 1, p. 23-31. http://dx.doi.org/10.4025/actasciagron.v33i1.5062.

ARNOLD, J. G.; SRINIVASAN, R.; MUTTIAH, R. S.; WILLIAMS, J. R. (1998). Large area hydrologic modeling and assessment part I: model development 1. JAWRA Journal of the American Water Resources Association, 34(1), 73-89. https://doi.org/10.1111/j.1752-1688.1998.tb05961.x.

ARNOLD, J. G.; WELTZ, M. A.; ALBERTS, E. E.; FLANAGAN, D. C. (1995). Chapter 8. Plant growth component. In U.S. Department of Agriculture (USDA) Water Erosion Prediction Project: Technical Report No.10, 8.1-8.41. West Lafayette, IN: USDA Agricultural Research Service National Soil Erosion Research Laboratory.

BAIER, W. (1978). Crop-weather models and their use in yield assessment. World Meteorological Organization (WMO) Tech. Note. In press. ISBN: 978-92-63-10458-8.

BAIER, W. (1979). Note on the terminology of crop-weather models. Agricultural Meteorology, v. 20, n. 2, p. 137-145. https://doi.org/10.1016/0002-1571(79)90032-3.

BERTRAM, Christine; REHDANZ, Katrin. (2015). The role of urban green space for human well-being. Ecological Economics, 120, 139-152. https://doi.org/10.1016/j.ecolecon.2015.10.013.

BOLUND, Per; HUNHAMMAR, Sven. (1999). Ecosystem services in urban areas. Ecological economics, v. 29, n° 2, p. 293-301. https://doi.org/10.1016/S0921-8009(99)00013-0.

BOOTE, Kenneth J.; JONES, James W.; WHITE, Jeffrey W.; ASSENG, Senthold; LIZASO, Jon I. (2013). Putting mechanisms into crop production models. Plant, cell & environment, 36(9), 1658-1672. https://doi.org/10.1111/pce.12119.

BORCHERT, Rolf. (1994). Soil and stem water storage determine phenology and distribution of tropical dry forest trees. Ecology 75, 1437–1449. https://doi.org/10.2307/1937467.

BOWLER, Diana E.; BUYUNG-ALI, Lisette M.; KNIGHT, Teri M.; PULLIN, Andrew S. (2010). A systematic review of evidence for the added benefits to health of exposure to natural environments. BMC public health, 10(1), 456. https://doi.org/10.1186/1471-2458-10-456.

BRAZIL – Brazilian Agricultural Research Company (EMBRAPA). Available in <http://www.cppse.embrapa.br/meteorologia/index.php?pg=inicio>, access on: May 20 2019.

BRAZIL – Brazilian Institute of Geography and Statistics (IBGE). (2010). **Cities**. Available on <https://censo2010.ibge.gov.br/sinopse/index.php?dados=29&uf=35>, access on: May 20 2019.

CHEN, J. M.: BLACK, T. A. (1992). Defining leaf area index for non-flat leaves. Plant Cell Environ. 15, 421–429.. https://doi.org/10.1111/j.1365-3040.1992.tb00992.x.

CHICKARMANE, Vijay; ROEDER, Adrienne H. K.; TARR, Paul T.; CUNHA, Alexandre; TOBIN, Corry; MEYEROWITZ, Elliot M. (2010). Computational morphodynamics: a modeling framework to understand plant growth. Annual review of plant biology, 61, 65-87. https://doi.org/10.1146/annurev-arplant-042809-112213.

CHIESURA, Anna. (2004). The role of urban parks for the sustainable city. Landscape and urban planning, v. 68, n. 1, p. 129-138. https://doi.org/10.1016/j.landurbplan.2003.08.003.

DELLA PERUTA, Raniero; KELLER, Armin; SCHULIN, Rainer. (2014). Sensitivity analysis, calibration and validation of EPIC for modelling soil phosphorus dynamics in Swiss agro-ecosystems. Environmental modelling & software 62 (2014): 97-111. https://doi.org/10.1016/j.envsoft.2014.08.018.

ESPARZA, A.; GOWDA, P.; BAUMHARDT, R.; MAREK, T.; HOWELL, T. (2007). Heat unit avail-ability for cotton production in the Ogallala Aquifer Region of the United States. The Journal of Cotton Science 11:110–117.

FOURCAUD, Thierry; ZHANG, Xiaopeng; STOKES, Alexia; LAMBERS, Hans; KÖRNER, Christian. (2008). Plant growth modelling and applications: the increasing importance of plant architecture in growth models. In: Annals of Botany, v. 101, nº 8, 2008, p. 1053-1063. https://doi.org/10.1093/aob/mcn050.

GILMORE, E. C.; ROGERS, J. S. (1958). Heat units as a method of measuring maturity in corn 1. Agronomy Journal, 50(10), 611-615. DOI: .2134/agronj1958.00021962005000100014x

HAN, M.; ZHAO, C.; ŠIMŮNEK, J.; FENG, G. (2015). Evaluating the impact of groundwater on cotton growth and root zone water balance using Hydrus-1D coupled with a crop growth model. Agricultural Water Management, 160, 64-75. https://doi.org/10.1016/j.agwat.2015.06.028.

HAQ, Shah Md. Atiqul. (2011). Urban green spaces and an integrative approach to sustainable environment. Journal of environmental protection, 2(05): 601. http://dx.doi.org/10.4236/jep.2011.25069.

HARGREAVES, G. H.; SAMANI, Z. A. (1985). Reference crop evapotranspiration from temperature. Applied engineering in agriculture, 1(2), 96-99. http://dx.doi.org/10.13031/2013.26773.

JOHNSON, I. R.; AMEZIANE, T. E.; THORNLEY, J. H. M. (1983). A model of grass growth. Annals of Botany, 51(5), 599-609. https://doi.org/10.1093/oxfordjournals.aob.a086506.

JOLLY, William M.; RUNNING, Steven W. (2004). Effects of precipitation and soil water potential on drought deciduous phenology in the Kalahari. Global Change Biology, 10(3), 303-308. https://doi.org/10.1046/j.1365-2486.2003.00701.x.

JONES, J. W.; HOOGENBOOM, G.; PORTER, C. H.; BOOTE, K. J.; BATCHELOR, W. D.; HUNT, L.A.; WILKENS, P. W.; SINGH, U.; GIJSMAN, A. J.; RITCHIE, J. T. (2003). DSSAT Cropping System Model. European Journal of Agronomy 18:235-265. https://doi.org/10.1016/S1161-0301(02)00107-7.

JOUVEN, M.; CARRÈRE, P.; BAUMONT, R. (2006). Model predicting dynamics of biomass, structure and digestibility of herbage in managed permanent pastures. 1. Model description. Grass Forage Sci. 61 (2), 112–124. https://doi.org/10.1111/j.1365-2494.2006.00515.x.

KACZYNSKI, Andrew T.; HENDERSON, Karla A. (2007). Environmental correlates of physical activity: a review of evidence about parks and recreation. Leisure sciences, 29(4), 315-354. DOI: https://doi.org/10.1080/01490400701394865.

KINIRY, J. R., BURSON, B. L.; EVERS, G. W.; WILLIAMS, J. R.; SANCHEZ, H.; WADE, C.; FEATHERSTON, J. W.; GREENWADE, J. (2007). Coastal bermudagrass, bahiagrass, and native range simulation at diverse sites in Texas. Agronomy Journal 99, no. 2, 2007: 450-461. https://doi.org/10.2134/agronj2006.0119.

KÖPPEN, W. P. (1931). Grundriss der Klimakunde. W. de Gruyter, Berlin.

LAFORTEZZA, Raffaele; CARRUS, Giuseppe; SANESI, Giovanni; DAVIES, Clive. (2009). Benefits and well-being perceived by people visiting green spaces in periods of heat stress. Urban Forestry & Urban Greening, 8(2), 97-108. https://doi.org/10.1016/j.ufug.2009.02.003.

LE ROUX, Xavier; LACOINTE, André; ESCOBAR-GUTIÉRREZ, Abraham; LE DIZÈSA, Séverine. (2001). Carbon-based models of individual tree growth: A critical appraisal. Annals of Forest Science 58.5, 469-506. https://doi.org/10.1051/forest:2001140.

LENTZ, W. (1998). Model applications in horticulture: a review. Scientia Horticulturae, 74(1-2), 151-174. https://doi.org/10.1016/S0304-4238(98)00085-5.

MAAS, Jolanda; VERHEIJ, Robert A.; GROENEWEGEN, Peter P.; DE VRIES, Sjerp; SPREEUWENBERG, Peter. (2006). Green space, urbanity, and health: how strong is the relation?. Journal of Epidemiology & Community Health, 60(7), 587-592. http://dx.doi.org/10.1136/jech.2005.043125.

MARCELIS, Leo F. M.; HEUVELINK, Ep; GOUDRIAAN, Jan. (1998). Modelling biomass production and yield of horticultural crops: a review. Scientia Horticulturae, 74(1-2), 83-111. https://doi.org/10.1016/S0304-4238(98)00083-1.

MCCOWN, R. L.; HAMMER, G. L.; HARGREAVES, J. N. G.; HOLZWORTH, D. P.; FREEBAIRN, D. M. (1996). APSIM: a novel software system for model development, model testing, and simulation in agricultural systems research. Agric. Syst. 50, 255/271. https://doi.org/10.1016/0308-521X(94)00055-V.

MCGREGOR, G. R.; NIEUWOLT, S. (1998). Tropical climatology: an introduction to the climates of the low latitudes (No. Ed. 2). John Wiley & Sons Ltd. ISBN : 0471966118.

MCMICHAEL, Anthony J. (2000). The urban environment and health in a world of increasing globalization: issues for developing countries. Bulletin of the World Health Organization, 78, 1117-1126.

MEDERSKI, H. J.; MILLER, M. E.; WEAVER, C. R. (1973). Accumulated Heat Units for Classifying Corn Hybrid Maturity 1. Agronomy Journal, 65(5), 743-747. https://doi.org/10.2134/agronj1973.00021962006500050020x.

MONSI, M; SAEKI, T. (1953). Uber den Lictfaktor in den Pflanzengesellschaften und sein Bedeutung fur die Stoffproduktion. Japan J. Bot. 14:22-52.

MONTEITH, John Lennox. (1977). Climate and the efficiency of crop production in Britain. Philosophical Transactions of the Royal Society of London B 281, 277–294. https://doi.org/10.1098/rstb.1977.0140.

MULLER, Bertrand; MARTRE, Pierre. (2019). Plant and crop simulation models: powerful tools to link physiology, genetics, and phenomics. Journal of Experimental Botany, Volume 70, Issue 9, 15 April 2019, Pages 2339–2344. https://doi.org/10.1093/jxb/erz175.

NEITSCH, S. L.; ARNOLD, J. G.; KINIRY, J. R.; WILLIAMS, J. R. (2011). Soil and water assessment tool theoretical documentation version 2009. Texas water resources institute. Texas AgriLife Research and USDA Agriculural Research Service, Temple, Texas, USA.

NOBRE, A. D.; CUARTAS, L. A.; HODNETT, M.; RENNÓ, C. D.; RODRIGUES, G.; SILVEIRA, A.; WATERLOO, M.;SALESKA, S. (2011). Height Above the Nearest Drainage–a hydrologically relevant new terrain model. Journal of Hydrology, 404(1-2), 13-29. https://doi.org/10.1016/j.jhydrol.2011.03.051.

NOWAK, David J.; CRANE, Daniel E.; STEVENS, Jack C. (2006). Air pollution removal by urban trees and shrubs in the United States. Urban forestry & urban greening, 4(3-4), 115-123. https://doi.org/10.1016/j.ufug.2006.01.007.

PAULEIT, Stephan; DUHME, Friedrich. (2000). Assessing the environmental performance of land cover types for urban planning. Landscape and urban planning, 52(1), 1-20. https://doi.org/10.1016/S0169-2046(00)00109-2.

PEDREIRA, Carlos G. S.; BROWN, R. H. (1996). Yield of selected and unselected bahiagrass populations at two cutting heights. Crop Sci. 36:134–137. https://doi.org/10.2135/cropsci1996.0011183X003600010024x.

PENG, S.; KRIEG, D. R.; HICKS, S. K. (1989). Cotton lint yield response to accumulated heat units and soil water supply. Field Crops Research, 19(4), 253-262. https://doi.org/10.1016/0378-4290(89)90097-X.

PIAO, Shilong; WANG, Xuhui; CIAIS, Philippe; ZHU, Biao; WANG, Tao; LIU, Jie. (2011). Changes in satellite-derived vegetation growth trend in temperate and boreal Eurasia from 1982 to 2006. Global Change Biology, v. 17, nº 10, p. 3228-3239. https://doi.org/10.1111/j.1365-2486.2011.02419.x.

RENNÓ, Camilo Daleles; NOBRE, Antonio Donato; CUARTAS, Luz Adriana; SOARES, João Vianei; HODNETT, Martin G.; TOMASELLA, Javier; WATERLOO, Maarten. (2008). HAND, a new terrain descriptor using SRTM-DEM: Mapping terra-firme rainforest environments in Amazonia. Remote Sensing of Environment, 112(9), 3469-3481. https://doi.org/10.1016/j.rse.2008.03.018.

RYMPH, Stuart J. Modeling growth and composition of perennial tropical forage grasses. PhD diss., University of Florida, 2004.

SÃO PAULO. Metropolitan Planning Company of São Paulo (EMPLASA). "Digital Surface Model (DSM) of Juqueriquerê River Basin." São Paulo: EMPLASA, No. 0973, 2013.

SCHAPENDONK, A. H. C. M.; STOL, W.; VAN KRAALINGEN, D. W. G.; BOUMAN, B. A. M. (1998). LINGRA, a sink/source model to simulate grassland productivity in Europe. European Journal of Agronomy, 9(2-3), 87-100. https://doi.org/10.1016/S1161-0301(98)00027-6.

STRAUCH, Michael; VOLK, Martin. (2013). SWAT plant growth modification for improved modeling of perennial vegetation in the tropics. Ecological Modelling, 269, 98-112. https://doi.org/10.1016/j.ecolmodel.2013.08.013.

TAO, Fulu; YOKOZAWA, Masayuki; ZHANG, Zhao. (2009). Modelling the impacts of weather and climate variability on crop productivity over a large area: A new process-based model development, optimization, and uncertainties analysis. Agricultural and Forest Meteorology, v. 149, p. 831–850. https://doi.org/10.1016/j.agrformet.2008.11.004.

TZOULAS, Konstantinos; KORPELA, Kalevi; VENN, Stephen; YLI-PELKONEN, Vesa; KAŹMIERCZAK, Aleksandra; NIEMELA, Jari; JAMES, Philip. (2007). Promoting ecosystem and human health in urban areas using Green Infrastructure: A literature review. Landscape and urban planning, 81(3), 167-178. https://doi.org/10.1016/j.landurbplan.2007.02.001

ULRICH, Roger S. (1983). Aesthetic and affective response to natural environment. Hum. Behav. Environ. Adv. Theory Res. 6, 85–125. https://doi.org/10.1007/978-1-4613-3539-9_4.

ULRICH, Roger S.; SIMONS, Robert F.; LOSITO, Barbara D.; FIORITO, Evelyn; MILES, Mark A.; ZELSON, Michael. (1991). Stress recovery during exposure to natural and urban environments. J. Environ. Psychol. 11 (3), 201–230. https://doi.org/10.1016/S0272-4944(05)80184-7.

UNITED NATIONS – UN, Department of Economic and Social Affairs, Population Division. World Urbanization Prospects: The 2014 Revision, 493p. 2015. Disponível em <https://esa.un.org/unpd/wup/Publications/Files/WUP2014-Report.pdf> Acesso em: 14 set. 2017.

WANG, Jen Yu. (1960). A critique of the heat unit approach to plant response studies. Ecology, 41(4), 785-790. https://doi.org/10.2307/1931815.

WATSON, D. J. (1947). Comparative physiological studies on growth of field crops. I. Variation in net assimilation rate and leaf area between species and varieties, and within and between years. Ann. Bot. 11, 41–76.

WILLIAMS, J. R.; JONES, C. A.; KINIRY, J. R.; SPANEL, D. A. (1989). The EPIC crop growth model. Transactions of the ASAE, 32(2), 497-0511. https://doi.org/10.13031/2013.31032.

WOLCH, Jennifer R.; BYRNE, Jason; NEWELL, Joshua P. (2014). Urban green space, public health, and environmental justice: The challenge of making cities 'just green enough'. Landscape and urban planning, 125, 234-244. https://doi.org/10.1016/j.landurbplan.2014.01.017.

ZAMAN, Mostafa Rezaei; MORID, Saeed; DELAVAR, Majid. (2016). Evaluating climate adaptation strategies on agricultural production in the Siminehrud catchment and inflow into Lake Urmia, Iran using SWAT within an OECD framework. Agricultural Systems, 147, 98-110. https://doi.org/10.1016/j.agsy.2016.06.001.

ZHANG, Xiaoyang.; FRIEDL, Mark A.; SCHAAF, Crystal B.; STRAHLER, Alan H.; LIU, Zhong. (2005). Monitoring the response of vegetation phenology to precipitation in Africa by coupling MODIS and TRMM instruments. Journal of Geophysical Research: Atmospheres, 110(D12). https://doi.org/10.1029/2004JD005263.

3. A GRASS GROWTH MODEL ADAPTED TO URBAN AREAS. PART 2: MODEL PERFORMANCE ASSESSMENT BASED ON LAI RETRIEVED FROM VEGETATION INDEXES

3.1. ABSTRACT

This paper presents a comparative analysis between the leaf area index (LAI) simulated by the model described in section 2 and the LAI retrieved from vegetation index (VI) from two different platforms, an unmanned aerial vehicle – UAV and PlanetScope imagery. Firstly, measurements of reflectance and leaf samples of bahiagrass (*Paspalum notatum* Flügge) were collected *in situ* and used as reference. Normalized difference vegetation index (NDVI), green normalized difference vegetation index (GNDI), and two-band enhanced vegetation index (EVI2) were calculated to estimate LAI using the ground-based data. EVI2 showed the best performance for this analysis and it was then applied to retrieve LAI from both the UAV and PlanetScope imagery. To evaluate the model performance, the associated determination coefficient (R^2) and root mean square error (RMSE) between LAI simulated into the model (default and adjusted) and LAI retrieved from both sensors are reported. The findings obtained in the analysis suggest that the proposed model is suitable for its purpose. However, some adjustments in the LAI curve development and in the dormant period are proposed.

Keywords: grass growth model; urban areas; LAI retrieval.

3.2. INTRODUCTION

Process-based plant models have significantly advanced with the development of computational science over the last decades. However, there are few references to vegetation growth models designed for urban areas (most of them are developed to simulate crop growth and yield). Thus, aiming to help government administrations with management and optimization of mowing processes of urban green areas – UGS (e.g. lawns, public parks squares, roadsides and around waterways), a grass growth model adapted to urban area conditions was implemented (section 2).

The model is designed to simulate the dynamics of leaf area index (LAI), biomass, evapotranspiration and soil water content, from local to large scales, going or not under mowing processes or not. However, only above-ground growth is modeled. The model presents two different approaches to trigger dormancy (from a daylength perspective or an annual soil moisture index – SMI). Phenological development is simulated based on daily cumulative heat units, biomass production is calculated using the light-use efficiency approach (MONTEITH, 1977), and plant growth constraints are controlled by stress factors. The model equations were either adapted from previous models (WILLIAMS et al. 1989; NEITSCH et al., 2011; SCHAPENDONK et al., 1998; KINIRY et al., 1992; JOUVEN, CARRÈRE, BAUMONT, 2006) or newly developed, as presented and discussed in section 2.

Plant development and health can be evaluated by LAI and biomass, which in turn can be estimated by either direct or indirect methods (GOWER, KUCHARIK, NORMAN, 1999). Direct measurements, which involve destructive sampling, can be time-consuming, labor-intensive, and are difficult to apply over large areas or for repeated measurements. On the other hand, indirect measurements, mainly based on remote sensing techniques, are non-destructive, cost-effective and faster (LIU, PATTEY, ADMIRAL, 2013; KROSS et al., 2015). One way to use remotely sensed data is through vegetation indices – VIs (KROSS et al., 2015).

VIs, or more generally spectral indices, have been successful used in studies of various biophysical vegetation variables, such as canopy cover, leaf area index (LAI), biomass, productivity, and absorbed photosynthetically active radiation – APAR (HATFIELD ET AL., 1984; ASRAR et al., 1984; SELLERS, 1985; ELVIDGE, CHEN, 1995; MYNENI, WILLIAMS, 1994; DAUGHTRY et al., 2000) regardless of the scale, going from ground leaf-level to aerial and orbital measurements (HALL et al. 1992; HALL, SELLERS, 1995; DAUGHTRY et al., 2000; GLENN et at., 2008; BERNI et al., 2009). In addition, the underwent development of VIs has allowed reliable spatial and temporal inter-comparisons of terrestrial photosynthetic activity and variations of LAI and canopy structure (HUETE et al. 2002; GOBRON et al., 1999; ZHU et al., 2013), which are critical to monitoring and modeling vegetation dynamics (ZHU et al., 2013). Thus, VIs may be now considered indispensable tools to environmental studies, such as climate and land-use-change detection, land cover classification and monitoring, among others (GLENN et at., 2008).

The Most commonly used VIs utilize red and near-infrared (NIR) canopy reflectance or radiance (HUETE, 1988), because of the unique properties exhibited by vegetation in these bands (BROGE, LEBLANC, 2000), i.e., an intense radiation absorption in the red wavelengths and a strong scattering/reflectance in the NIR region (GOBRON et al., 1999). Ratio indices involve linear combinations of Photosynthetically Active Radiation (PAR) and NIR bands against another linear set of the same bands (TUCKER, 1979; HUETE, JACKSON, POST, 1985; BROGE, LEBLANC, 2000). The normalized difference vegetation index (NDVI – ROUSE, 1974), soil adjusted vegetation index (SAVI – HUETE, 1988), enhanced vegetation index (EVI – HUETE et al, 2002), two-band enhanced vegetation index (EVI2 – JIANG et al., 2008), and green normalized difference vegetation index (GNDVI – GITELSON, MERZLYAK, LICHTENTHALER, 1996) are some examples of well-established VIs.

Thus, the goal of this work is to assess the performance of the model by comparing the LAI simulated by the previously proposed model (section 2) to the LAI retrieved from VIs, which was assumed to be a proxy of the "effective" or "true" LAI (LAI_e) obtained from destructive samplings. This paper is structured as follows: in Section 3.3, we introduce the model functioning, the application of VIs as a tool for LAI retrieving, and the data source and processing. In Section 3.4, the simulated and retrieved LAI are described, and the results are discussed. Lastly, we present the conclusions of this study in Section 3.5.

3.3. MATERIAL AND METHODS

3.3.1. Model functioning

The model was developed in Phyton 3.7, a user-friendly open-source and high-level programming language. It runs at a daily time-step with two scenarios, optimal and actual conditions, and the main outputs are LAI and biomass. The model is capable of simulating growth for both annual and perennial plants. Since there are no records for the nutrient content in urban area soils, the model neither estimates the nutrient uptake by plants nor its potential stress in the areas of interests (UGS). Three daily stresses conditions are used: stress caused by temperature, water available in the soil, and solar radiation. The required model inputs are (I) the maximum LAI for the considered species, (II) the plant's minimal (base), optimal and

maximum temperatures for growth, (III) the light extinction coefficient, (IV) the potential heat units required for maturity, (V) field capacity for the site (when it is unknown, the model estimates this value from runoff curve number method [CN] and LAI), (VI) the weather data for the simulated period (solar radiation, temperature, precipitation, and reference evapotranspiration [when not provided, the model estimates it according to Hargreaves method]), and (VII) mowing regime based on specific dates or a user-defined maximum LAI value. The model resets the growth cycle after the regular mowing processes.

3.3.2. LAI retrieval and model performance

As already extensively suggested in the literature, LAI can be retrieved from VIs (see KROSS et al., 2015; TOWERS, STREVER, POBLETE-ECHEVERRÍA, 2019, and other references therein). Thus, to assess the performance of the model, this work uses the comparison between the LAI simulated in the model and the LAI retrieved from remotely sensed VIs, which were assumed to be a proxy of the effective LAI. Given that the model requires many variables that are intrinsic to each vegetation species, bahiagrass (*Paspalum notatum* Flügge) was selected as reference, since it is one of the most grown species in urban public areas in Brazil, especially in lawns, and public parks and squares.

For the LAI retrieval, we firstly focused on gathering the spectral response (reflectance) *in situ* and measuring the effective LAI (LAI_e) using the destructive approach, which is better described in the next section. Then, NDVI, GNDVI, and EVI2 performance were evaluated (Table 4).

Table 4: Vegetative indices evaluated in this study

Index	Equation	Bands applied	Reference
NDVI	$\dfrac{(\rho_{NIR} - \rho_{\text{red}})}{(\rho_{NIR} + \rho_{\text{red}})}$	660 nm (red) 800 nm (NIR)	Tucker (1979)
GNDVI	$\dfrac{(\rho_{NIR} - \rho_{\text{green}})}{(\rho_{NIR} + \rho_{\text{green}})}$	550 nm (green) 800 nm (NIR)	Gitelson et al. (1996)
EVI2	$\dfrac{2.5 \times (\rho_{NIR} - \rho_{\text{red}})}{(\rho_{NIR} + 2.4 \times \rho_{\text{red}} + 1)}$	660 nm (red) 800 nm (NIR)	Jiang et al. (2008)

Afterward, the index with the highest explanatory power against effective LAI was selected to be used on the LAI retrieval from the VIs derived from sensors of two different platforms, an unmanned aerial vehicle – UAV and PlanetScope imagery (from www.planet.com). This data acquisition is described in section 3.3.2.2. Once the LAI retrieved from both sensors were obtained, they were compared to the LAI simulated in the model.

3.3.2.1. *Reference sampling of LAI and reflectance signature*

Field reference data were collected in an open area composed mainly by bahiagrass located next to the Department of Environmental Science of Federal University of Sao Carlos (UFSCar), state of Sao Paulo, Brazil. This area was selected because it goes through regular mowing processes and was easy to keep in track.

The data acquisition took place in May of 2018 and April of 2019, at which spectral signature and leaf sampling were collected (Table 5). 13 circular sites of 0.165 m^2, randomly distributed over the site, were selected (Fig. 16a). After gathering the reflectance response, we harvested the spots and leaf area measurements were performed in the laboratory later. Photos of the leaves were taken with a Canon EOS 750D (Canon Inc.) camera and processed by using ImageJ software (SCHINDELIN et al., 2012) to estimate the effective LAI (LAI_e), in a procedure similar to Martin et al. (2013). This LAI was set as reference in the retrieval of LAI (Fig. 16b).

Canopy reflectance measurements were made before harvesting the leaves by using the portable analytical spectral device (ASD) Field-Spec 4 Hi-Res spectroradiometer (Fig.17). The ASD FieldSpec measures spectral signature over the 350 – 2500 nm region (2151 spectral channels) with a sampling interval of 1.4nm between 350-1000nm. Bandwidth is 3 nm in the visible (VIS) and NIR and 8 nm in the short-wave infrared (SWIR). The measurements were made from about 1.15 m above the plot and a probe with 8°of a field of view (FOV) was used. As a result, at the plot level, a circular area of about 0.02 m^2 was measured and each measurement represents the average of 6 readings at the same spot. Canopy reflectance was measured between 01:00 p.m. and 03:30 p.m, in clear sky conditions. Calibration was done by using a white Spectralon panel® (Labsphere, Inc., North Sutton, NH). The reflectance signature

for the 13 sites is shown in Fig. 17, which also indicates the spectral bands used to calculate the VIs.

Table 5: Dates of ground-based data acquisition

	MAY 2018			APRIL 2019
	25th	30th	31st	24th
Sample	1, 2, 3 and 4	5 and 6	7, 8, 9, 10, 11 and 12	13

Figure 16: (a) the view angle (80º) of the ASD FieldSpec measurements above one of the circular sites; (b) Example of photographs taken in the experiment for leaf area estimation by ImageJ software.
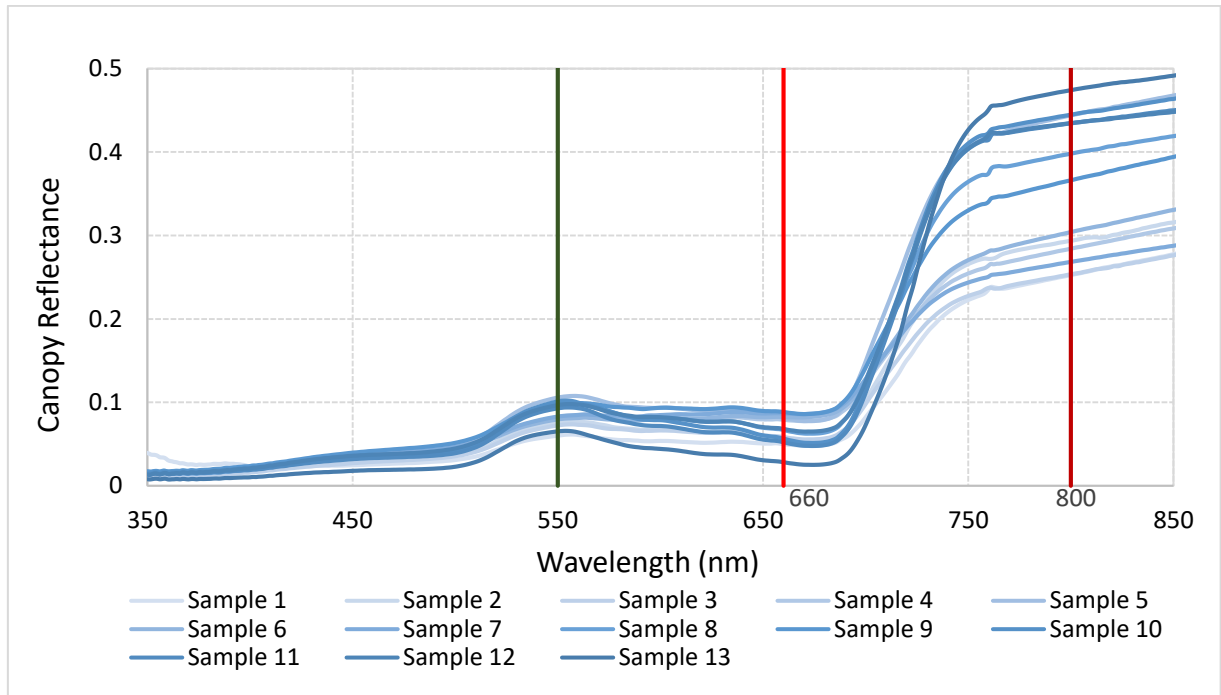
Figure 17: The canopy reflectance (from 350 to 850 nm) of the 13 sites were obtained by the average of 6 readings at each spot. The vertical lines represent the green (550 nm), red (660 nm) and NIR (800 nm) wavelength used to calculate the VI.

3.3.2.2. Image acquisition and processing

As stated before, the VIs were also generated with imagery from two different platforms: collected with a UAV and from PlanetScope CubeSats. The UAV platform used in this study was a DJI Phantom 4 quadcopter (Shenzhen, China), equipped with a multispectral MAPIR Survey 3N RGN (MAPIR) camera equipped with an onboard GPS (Table 6). The MAPIR camera captures light in the green (550 nm), red (660 nm), and near-infrared (850 nm) wavelengths. The images are produced in JPG and RAW + JPG format with dimensions of 4000 × 3000 pixels, with a ground sample distance (GSD) of 2.3 cm/px at 120 m. The MAPIR has a faster interval timer, 1.5 seconds for JPG mode and 2.8 seconds for RAW + JPG mode, which not only reduces the flight time but also enables higher overlapping (MAPIR, 2018). For the study, images overlap was sufficient to produce reasonable orthomosaics with a resolution of 1 cm/px.

Table 6: Specifications of Phantom 4 Professional aircraft and MAPIR Survey 3N RGN camera used in the UAV missions.

Phantom 4	
Weight (Battery & Propellers Included)	1380g
Flight time	Approx. 28 min
Max. speed	20 m/s (S-mode, no wind)
Max. flight altitude	6000 m
Operating temperature range	0° to 40°C
MAPIR Survey 3N RGN	
Image size	4000 × 3000 (12MP)
	3264 × 2448 (8MP)
Filter Transmission	RGN (Red+Green+NIR): 550nm/660nm/850nm
Image format	RAW (12bit) + JPG (24bit), JPG (24bit)
Lens	41° f/3.0
GSD	2.3 cm/pixel – 120 AGL
Sensor	Sony Exmor R IMX 117 12MP (Bayer RGB)
Photo interval	1.5 s/JPG, 2.8 s/RAW+JPG
ISO range	50 – 1600
GPS/GNSS	ublox UBX-G7020-KT

A total of 11 flights were performed in the same area mentioned earlier, in the period from March to July of 2019, between 11:30 a.m. and 02:00 p.m., in clear sky conditions, and in flying altitude of 30 m (Table 7; Fig. 18). The first flight was carried out a couple of days after a mowing process, which allows one to assume this as a scenario with the smallest LAI value. A calibration target with white, grey and black patches was placed on the ground in a position to ensure to be a part of the final image mosaics, allowing the forward reflectance equalization. All Phantom missions, including takeoff and landing, were fully controlled by an autopilot system (the DroneDeploy software), with the same flight paths based on GPS waypoints programmed before the missions. The imagery taken by MAPIR were first processed and calibrated with MAPIR Camera Control application (MAPIR, 2019). Then, orthomosaics were generated with Agisoft Metashape software and, finally, ArcGIS Pro (version 2.4,

Environmental Systems Research Institute, Redlands, CA, USA) was used for geospatial processing.

Table 7: Dates of UAV Phantom 4 flight.

2019
30 March
11, 18 and 30 April
20, 22, 27 and 29 May
5 June
11 and 12 July

Finally, imagery from the same region were acquired from the PlanetScope (PS), which is a constellation of small and standardized satellites, which are commercially operated by Planet Labs (or only Planet). Planet is an aerospace and data analytics company, which now runs the largest constellation of Earth imaging satellites (HOUBORG, MCCABE 2018). The PS constellation currently consists of approximately 130 active 3U (i.e., 10 x 10 x 30 cm) CubeSats with a mass around 4 kg, which are able to provide daily nadir-pointing land surface imaging of the entire Earth (PLANET, 2019).

The PS constellation of CubeSats, so-called "Doves", captures images at a spatial resolution of approximately 3 m (GSD) in four spectral bands, red (590 – 670 nm), green (500 – 590 nm), blue (455 – 515 nm), and near-infrared – NIR (780 – 860 nm). The PS nanosatellites are deployed into two different orbital configurations. Some of the CubeSats operate in International Space Station orbits, with an altitude of approximately 400 km, a variable equatorial crossing time and a GSD of approximately 3 m. Meanwhile, most of them are deployed into sun-synchronous orbits (approximately 475 km orbit altitude) with Equator crossing time between 9:30 – 11:30 a.m. (local solar time) and a nadir GSD of 3.7 m (Table 8).
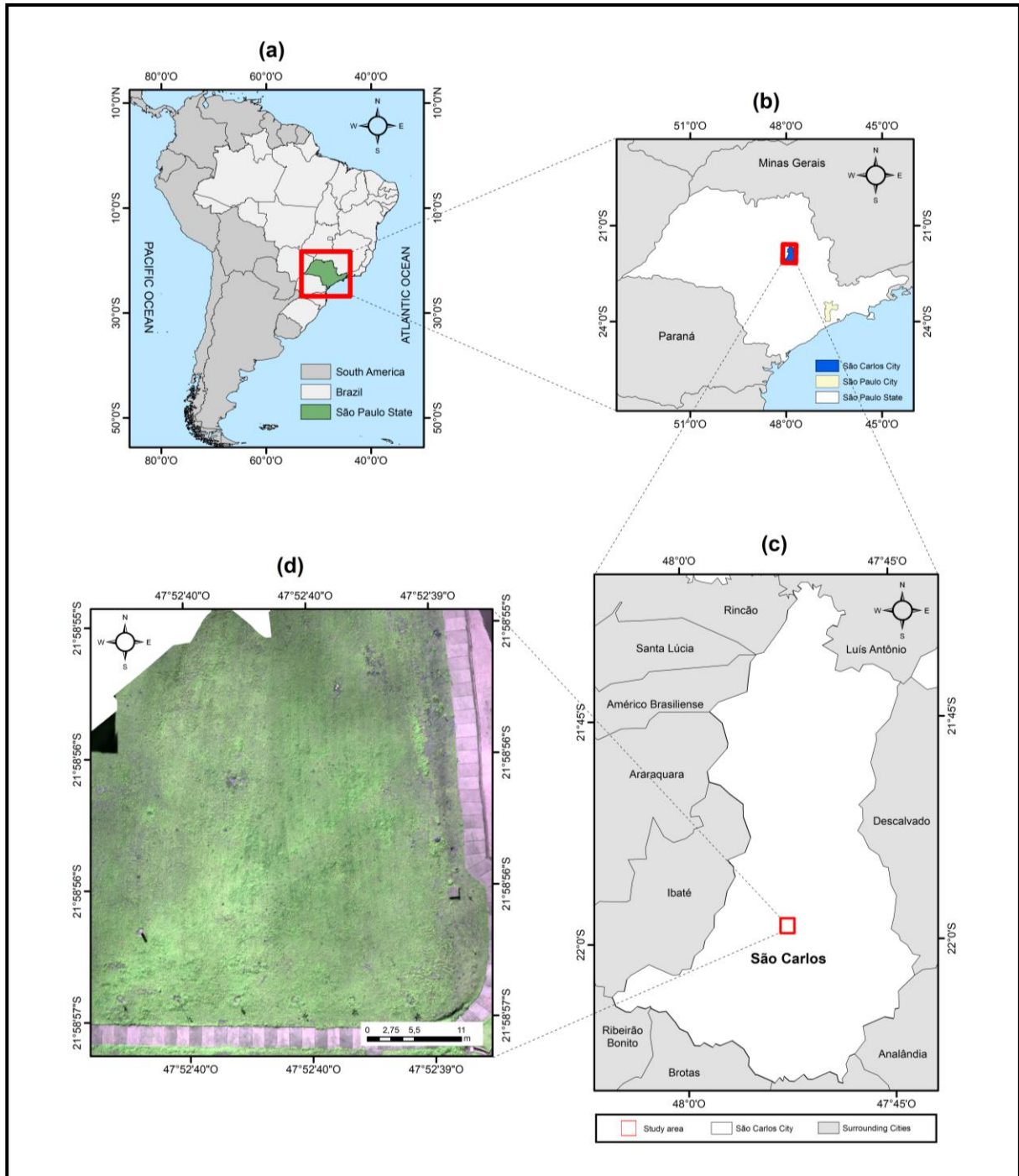
Figure 18: Location of the study area. It is presented an RGB composition (false color) from MAPIR camera in the bottom left corner (d). For the VIs calculations from both sensors, the average value inside the red rectangle was considered.

Table 8: PlanetScope CubeSat constellation and sensor specifications

	International Space Station Orbit	**Sun-synchronous Orbit**
Orbit Altitude (reference)	400 km (51.6° inclination)	475 km (98° inclination approx.)
Max/min latitude coverage	± 52° (depending on season)	± 81.5° (depending on season)
Equator crossing time	variable	9:30 – 11:30 am (local solar time)
Sensor type	Three-band frame Imager or four-band frame Imager with a split-frame NIR filter	Three-band frame Imager or four-band frame Imager with a split-frame NIR filter
Spectral bands	Blue: 455 - 515 nm Green: 500 - 590 nm Red: 590 - 670 nm NIR: 780 - 860 nm	Blue: 455 - 515 nm Green: 500 - 590 nm Red: 590 - 670 nm NIR: 780 - 860 nm
Ground sample distance (nadir)	3.0 m (approx.)	3.7 m
Frame size	20 km x 12 km (approx.)	24.6 km x 16.4 km (approx.)
Camera dynamic range	12-bit	12-bit

A total of 170 clipped PlanetScope Ortho Tiles encompassing the study area were downloaded using the "Explorer" online application (https://www.planet.com/explorer/), in the period between October of 2017 and June of 2019 (Table 9). To avoid potential uncertainties and any cloud contamination, only cloud-free images were selected. According to Planet, atmospheric and radiometric corrections were applied to all imagery, however, it may be possible that the images still present some limitations despite the corrections. All images downloaded PS-clipped TIFFs were processed with ESRI ArcGIS Pro afterward. After all data acquisition and processing, the calculation of the three VIs was performed: NDVI, GNDVI, and EVI2. From the resulting images, the average values of each VI were obtained from all images (UAV and PS constellation) and within a defined area, as shown by the polygon in Figure 17. Lastly, the LAI retrieved from the VI of both sensors was compared the LAI simulated in the model, and the associated determination coefficient (R^2) and root mean square error (RMSE) were reported.

Table 9: Dates of PlanetScope imagery acquisition in the period between 2018 and 2019.

2017		
month	**number of images**	**day**
October	8	6, 10, 12, 13, 15, 16, 17 and 24
November	5	12, 16, 17, 24 and 29
December	7	5, 9, 13, 15, 16, 29 and 26

2018		
month	**number of images**	**day**
January	3	4, 20 and 24
February	7	1, 3, 8, 9, 16, 23 and 28
March	12	4, 5, 6, 14, 17, 18, 19, 23, 24, 25, 27 and 28
April	11	6, 9, 10, 13, 17, 19, 23, 25, 26, 27 and 28
May	17	2, 5, 6, 7, 10, 11, 14, 20, 21, 22, 23, 24, 26, 27, 28, 30 and 31
June	7	15, 17, 21, 26, 27, 29 and 30
July	14	2, 5, 9, 11, 14, 16, 18, 19, 22, 24, 25, 27, 29 and 30
August	11	8, 11, 13, 14, 19, 20, 24, 27, 28, 29 and 31
September	9	6, 8, 9, 10, 11, 13, 24 and 25
October	9	2, 3, 12, 16, 20, 21, 22, 28 and 30
November	2	27 and 29
December	3	7, 13 and 15

2019		
month	**number of images**	**day**
January	7	3, 7, 15, 18, 28, 29 and 31
February	2	9 and 23
March	5	13, 23, 26, 28 and 31
April	11	2, 4, 10, 12, 18, 19, 20, 21, 22, 26 and 28
May	6	7, 9, 13, 22, 27 and 30
June	14	6, 7, 8, 9, 12, 14, 18, 22, 23, 24, 26, 28, 29 and 30

3.4. RESULTS AND DISCUSSION

3.4.1. VIs sensitivity to LAI changes

The effective LAI (LAI$_e$; $n = 13$) measured by destructive sampling and its respective reflectance in blue, green, red and NIR channels are presented in Table 10. The LAI$_e$ values ranged from 0.68 to 2.6. The relationship between NDVI, GNDVI, and EVI2 derived from the ground-based measurements and the effective LAI based on a linear regression is presented in Fig. 19 in terms of R^2 and RMSE of the linear regression for their relationship with LAI$_e$. In the experiment used as reference, NDVI, GNDVI, and EVI2 achieved R^2 values of 0.52, 0.56, and 0.75, respectively. In the same sense, RMSE values are of 0.37 for NDVI, 0.35 for GNDVI, and 0.27 for EVI2.

Table 10: The effective LAI (LAI_e) from destructive measurements and its respective reflectance in blue, green, red and NIR bands gathered from ASD FieldSpec.

| Sample	Date	LAI$_e$	REFLECTANCE			
			Blue 460 nm	Green 550 nm	Red 680 nm	NIR 800 nm
1	25 May 2018	0.68	0.025	0.060	0.049	0.252
2	25 May 2018	0.88	0.031	0.076	0.055	0.293
3	25 May 2018	0.96	0.028	0.072	0.057	0.253
4	25 May 2018	1.49	0.035	0.082	0.080	0.284
5	30 May 2018	1.71	0.037	0.105	0.079	0.444
6	30 May 2018	0.97	0.035	0.078	0.084	0.304
7	31 May 2018	1.05	0.037	0.083	0.088	0.268
8	31 May 2018	1.88	0.035	0.096	0.064	0.398
9	31 May 2018	1.24	0.042	0.098	0.088	0.366
10	31 May 2018	1.81	0.037	0.101	0.052	0.445
11	31 May 2018	1.60	0.033	0.093	0.049	0.434
12	31 May 2018	2.11	0.037	0.097	0.066	0.435
13	27 April 2019	2.60	0.019	0.065	0.026	0.474
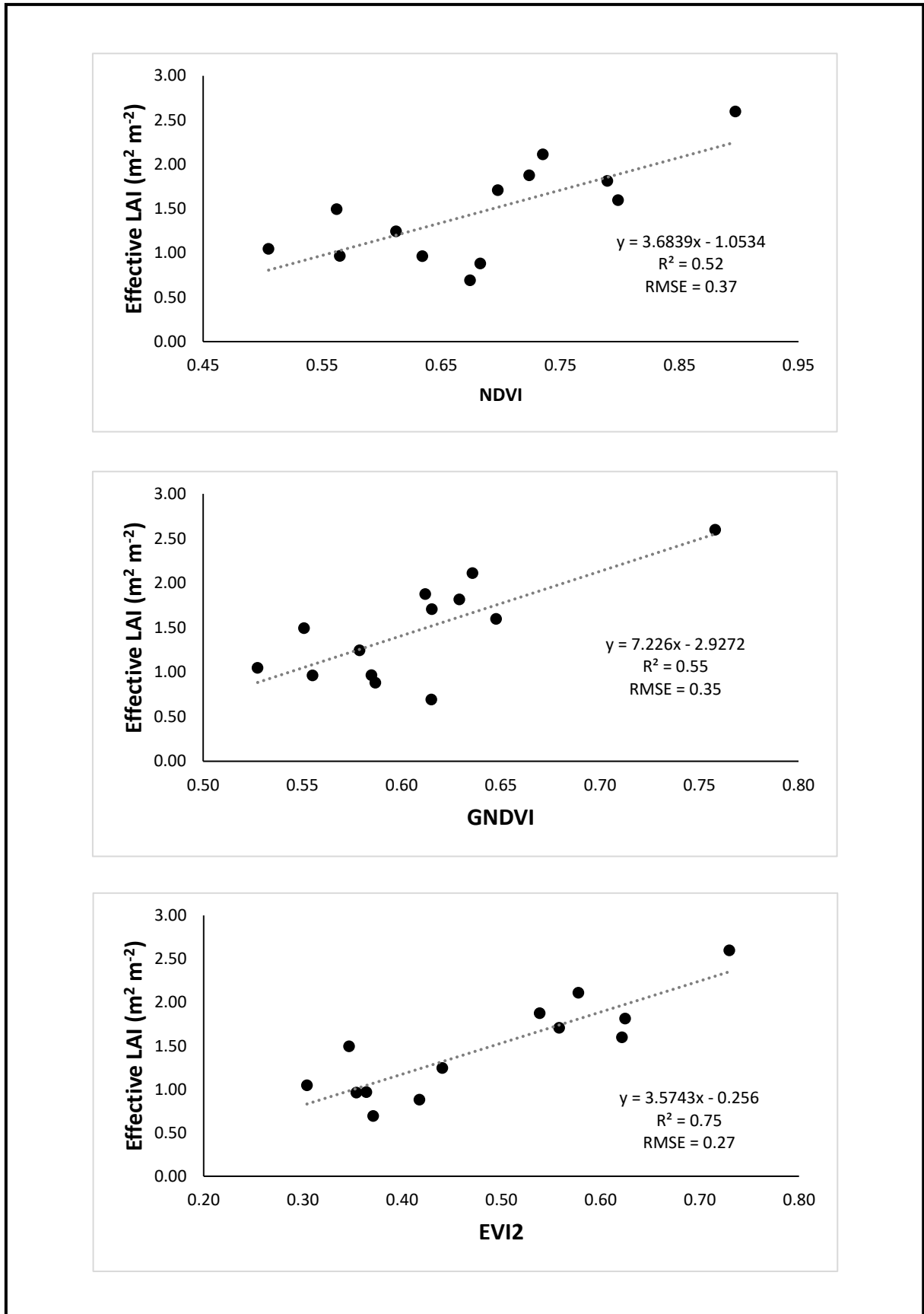
Figure 19: NDVI, GNDVI, and EVI2 performances for LAI retrieval from ground-based measurements.

In this study, the agreement between the VIs and LAI was not as high as described in previous works (e.g. DARVISHZADEH et al., 2011; XIE et al., 2014; TOWERS, STREVER, POBLETE-ECHEVERRÍA, 2019), which may be related to the fact that only 13 ground samples were collected and analyzed. It is also important to point out that since there were no LAI samples lower than 0.6, it is possible that additional measurements of LAI could lead to more suitable than they are at this moment. Despite that, since EVI2 showed the highest sensitivity to LAI changes, it was selected to be performed in the LAI retrieval for MAPIR Survey 3N and PlanetScope imagery, which will be later used to evaluate the model performance for LAI simulation.

3.4.2. EVI2 from MAPIR Survey 3N and PlanetScope imagery

EVI2 index was generated for the imagery from both sensors, MAPIR (11 images) and PS (32 images), for the period from 30 of March of 2019 to 12 of July 2019, to thus compare their results (Fig. 20). It is important to highlight that the values were averaged over the study area returning a single value for each image (Fig. 18). EVI2 from MAPIR ranged from 0.29 to 0.56, while EVI2 from PS ranged from 0.22 to 0.72. There were two mowing processes for the interval under consideration, the first one was done on March 27 (three days before the first image acquired), and the second one was performed on May 28. A small decline of EVI2 was observed for MAPIR on the following days right after the second mowing process (between May 29 and June 5), which may have been caused by the hay on the ground. As there are more images for this sensor than for PS during this period, it is harder to compare the sensibility of both sensors for this situation. On the other hand, this behavior was not observed after the first mowing process, which may be justified by the fact that the hay could have been removed by the cleaners.

EVI2 from PlanetScope shows higher values and variations than based on MAPIR, which may be resulted from the difference in the spatial and radiometric resolutions of the sensors or even due to some noise/disturbance in the image generation. However, in general, both sensors present similar trends for EVI2 derivation, i.e. they show an increase, decrement, or stability for the same periods. Furthermore, following the data presented in Fig. 20, precipitation appears to be strongly related to the development of the plant (grass in this case). Dividing the period analyzed into 2 parts according to the mowing processes, it may be

affirmed that the growth cycle in the second part was possibly affected by the drought in June, while it did not occur after the first mowing since there were enough rainfalls during the beginning of the cycle. In addition, June is in the early winter, which means lower temperatures and a natural reduction in vegetation growth.
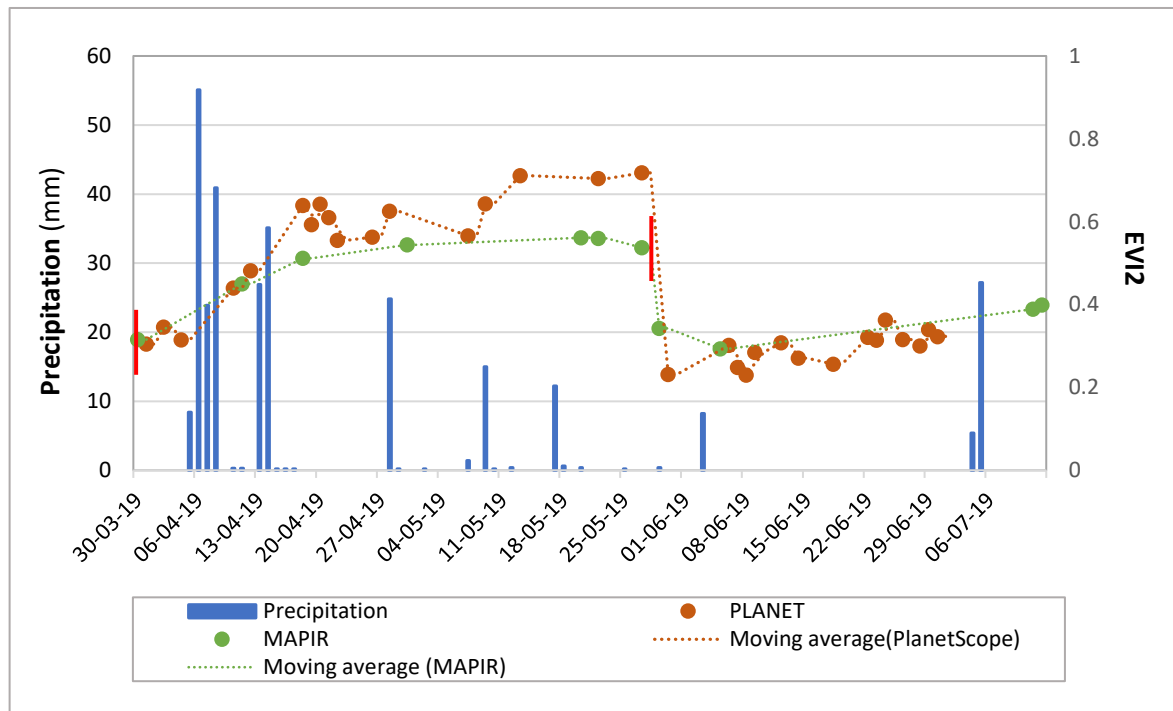

Figure 20: EVI2 calculated for MAPIR and PlanetScope for the period between 30 April 2019 and 12 July 2019, and the precipitation for the same period. Right axis shows the VIs values and left axis the precipitation. The red vertical lines represent the mowing processes.

For a more effective analysis, EVI2 for the PlanetScope imagery ($n = 170$) was created for the period from October of 2017 to June of 2019 (Fig. 21). This analysis sought to create a representation for a whole growth cycle (from September of 2018 to May of 2019) as well as for the dormant period (June, July, and August of 2018). In addition, the analysis of some months before the cycles under interest is also presented as an attempt to identify some possible variations in the growth cycle and patterns in the mowing intervals.
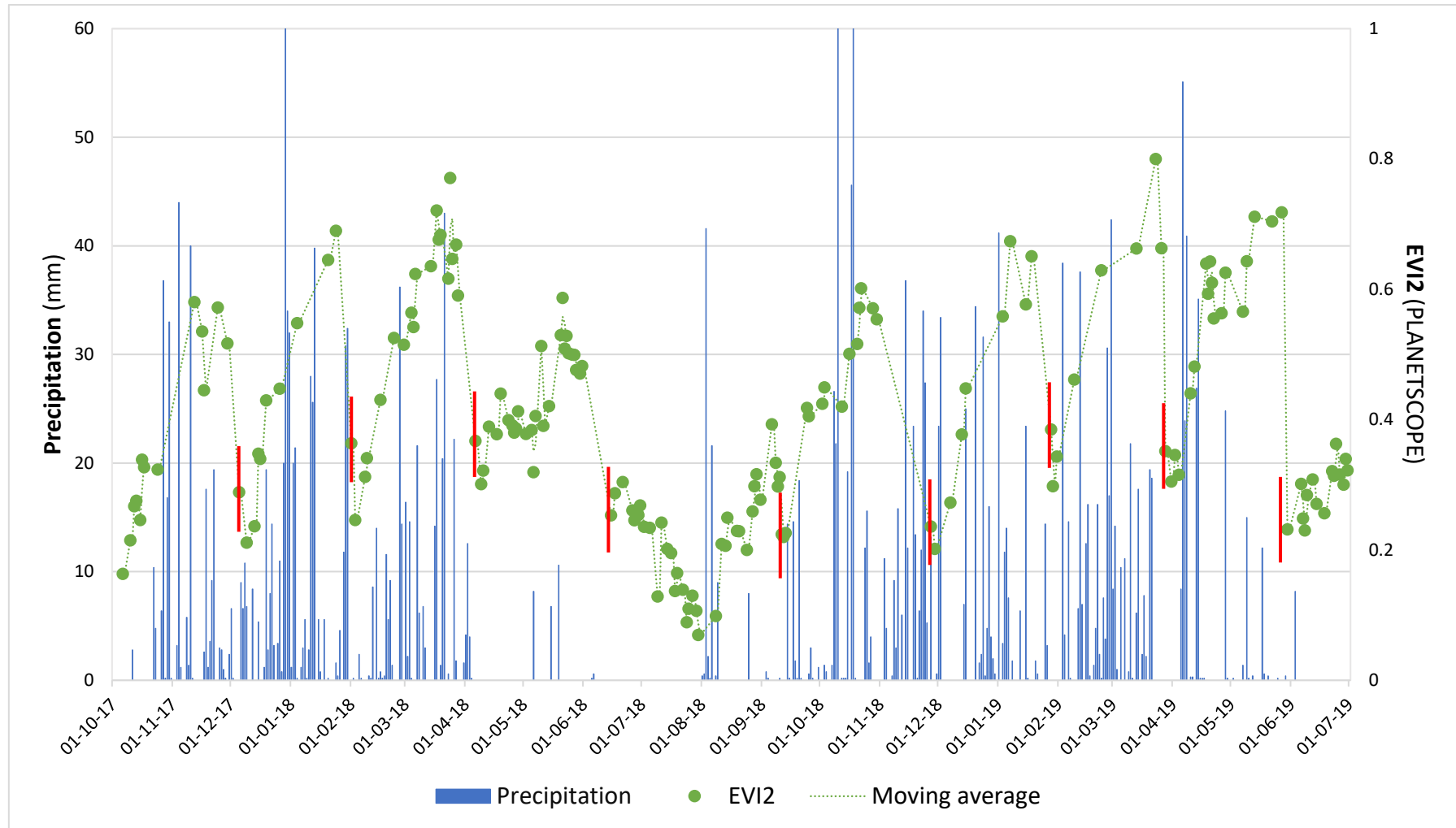
Figure 21: Times series of EVI2 calculated from PlanetScope CubeSats from October of 2017 to June of 2019 and the precipitation for the same period. The red vertical lines represent the approximate dates for the mowing processes.

For the analyzed presented, the index based on PS imagery ranged from 0.06 to 0.80, with the maximum value in the growth cycle and the minimum in dormancy, respectively. EVI2 showed an (expected) considerable decrease during the dormant period (from 1st of June to 31st of July of 2018), followed by a slight increase at the end of dormancy (1st of August), which was not expected. This finding seems to be closely related to the precipitation for this period. Stable or decreasing periods regarding EVI2 values, regardless of the mowing processes, may have been driven by droughts (not only).

Lastly, 9 mowing processes were identified with intervals ranging from 58 to 77 days during the growth cycle (September to April). As the exact dates are unknown, the dates indicating the beginning of a new growth cycle in the model were defined based on the images (Table 11). A little decrement of the index was identified after some mows as well, which may be an effect of the hay that remains on the ground after the mowiing process.

Table 11: More likely dates for growing processes identified in the imagery.

1	5 December 2017
2	1 February 2018
3	6 April 2018
4	15 June 2018
5	11 September 2018
6	27 November 2018
7	28 January 2019
8	27 March 2019
9	28 May 2019*

*according to the MAPIR images (see Fig. 20)

3.4.3. LAI retrieval and model performance assessment

As mentioned before, the model performance was assessed comparing the LAI simulated by the model with the LAI retrieved from the imagery from both sensors (Fig. 22). In a first moment, the model was run considering bahiagrass requirements for growth based on

the literature (called here as 'default simulation'). The model simulation started on 5 December of 2017 and lasted until on 27 May of 2019. Seven growth cycles were simulated during what was considered the growth period (September to May). However, the mowing process identified in June of 2018 was not simulated in the model, once it was in the dormant period (the model simulates the LAI decrement for this period). Such conditions still need to be implemented in the model. On the other hand, the LAI retrieval was generated applying the linear regression from EVI2 to LAI for Survey and PS imagery, as described early.

It should be noted that the images after the mowing process on May 28 were excluded, thus a total of 142 images from PS and 7 images from MAPIR were performed. The values of the retrieved LAI varied from 0 to 2.60 for PS whilst it ranged from 0.79 to 1.75 for MAPIR. On the other side, the LAI simulated in the model ranged from 0.50 to 1.90. It is important to emphasize that both the minimum LAI to begin the growth cycle and the minimum value at the end of dormancy was set to 0.50 (according to *in situ* samplings this is the minimum LAI for bahiagrass after mowing).

The LAI retrieved from PS imagery showed higher values compared to the LAI from MAPIR. In addition, it also showed LAI equal to zero (i.e. the complete death of the biomass) during the dormant period (from May to July of 2018), which is quite unlikely, since this behavior was not observed in the area of interest. One possibility, in this case, is that the EVI2 from the PS imagery does not present a good sensibility for LAI changes in lower (< 0.5) and higher (>2.0) values. It is possible that the linear regression does not give a good representation of these intervals as well. On the other hand, a considerable part of LAI retrieval from MAPIR and PS shows similar values and behavior, regardless of some oscillations and high values from PS. A direct correlation between MAPIR and PS could not be performed, since there are only three images for the same date for both sensors (18 April, and 22 and 27 May of 2019).

Based on the parameters defined in the literature, it was observed that the LAI cycle simulated by the model did not follow as closely as expected the LAI based on EVI2 curve. Given that, some adjustments were made in the leaf area development curve (see equations 2.24, 25 and 26) to approximate the model simulation to the retrieved LAI. Only the shape coefficients were modified. This scenario was called as model-adjusted (Fig. 22).
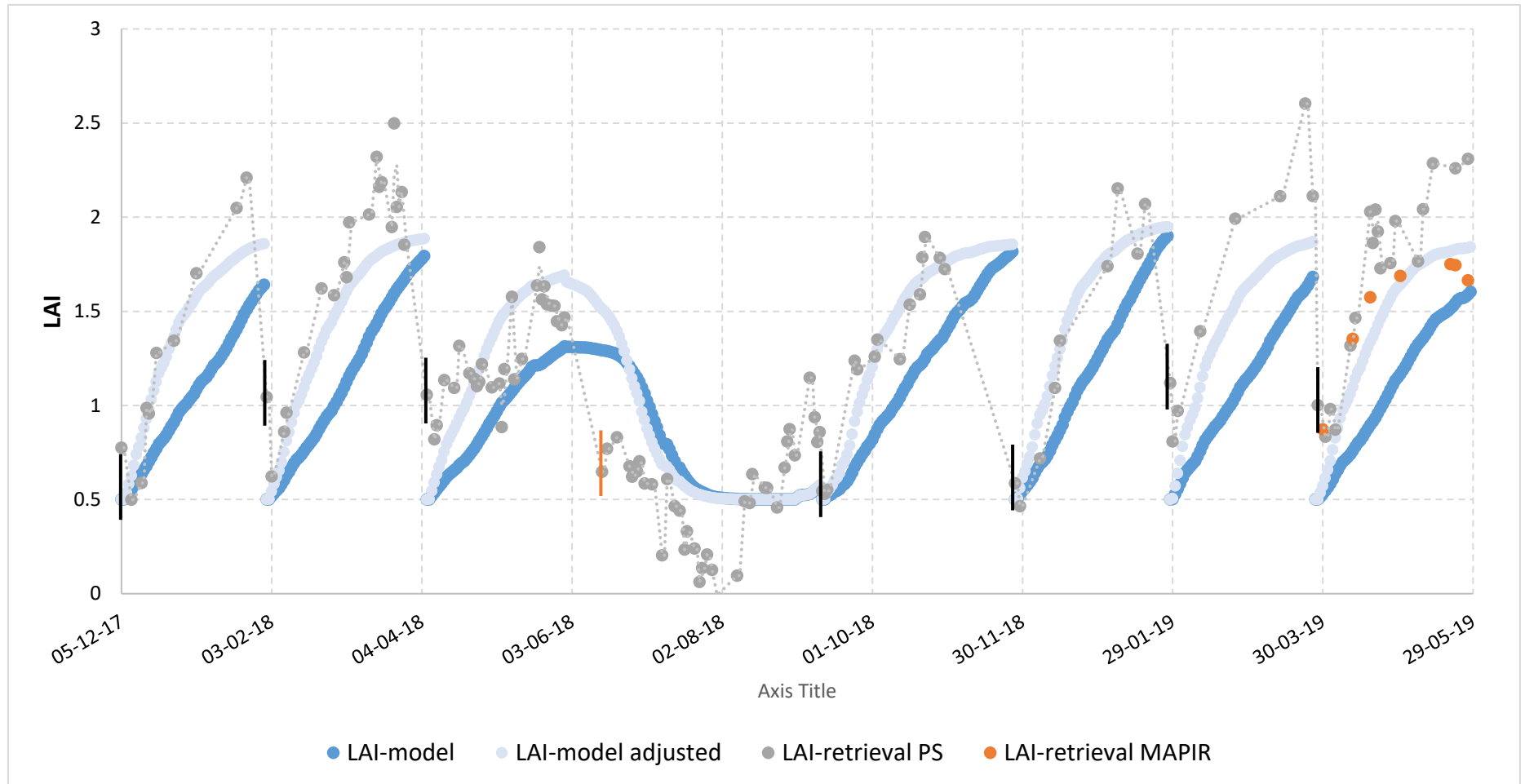
Figure 22: LAI retrieval from MAPIR (orange) and PS (gray) imagery, LAI simulated in the model using parameters from literature (dark blue), and LAI simulated in the model adopting LAI retrieval from MAPIR as reference (light blue). The black vertical lines represent the beginning of a new growth cycle. The orange vertical line represents the mowing process, that was not simulated in the model.

The model-adjusted LAI ranged from 0.50 to 1.95 and, compared to the default simulation, the former showed slightly higher maximum values for most of the growth cycles. However, the difference was only significantly bigger in the period from April to May of 2018. Furthermore, it seems that the adjusted simulation shows a better representation of growth cycles for a long-period simulation, regarding the development curve of the LAI retrieved from PS imagery.

A simple comparison of the values simulated in the model to the LAI retrieved from PS and MAPIR suggest that the last present a better correlation with the values from the model, but it is worth noting that the sample collection of MAPIR is much less that of PS (Fig. 23). The values obtained from the model-adjusted simulation presented a better correlation for both sensors comparing to the default mode, R^2 of 0.93 and RMSE of 0.19 for LAI retrieved from MAPIR, and R^2 of 0.74 and RMSE of 0.32 for LAI retrieved from PS.
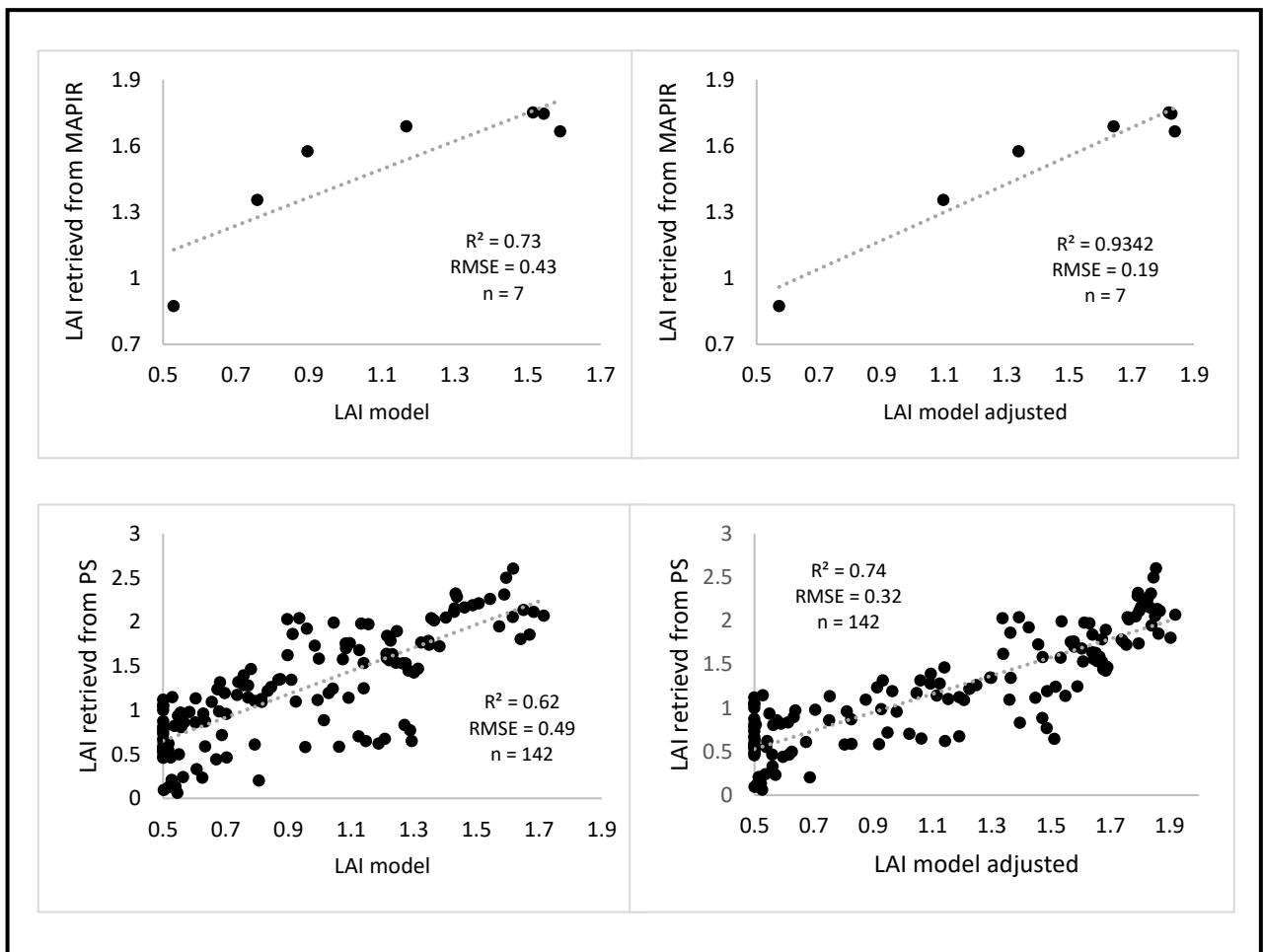

Figure 23: LAI retrieved from both sensors versus LAI from the model (default and adjusted) with R^2, RMSE and sample collection (n).

It is also worth to mention, however, that the LAI retrieved from both UAV and satellite imagery depends on the model defined with *in situ* measurements, which is based on a reduced sampling. Thus, more data would be necessary to confirm the appropriateness of the fitted model.

3.5. CONCLUSIONS

The performance of LAI simulation obtained from the model proposed in Section 2 was evaluated based on the LAI retrieved from UAV and PlanetScope imagery. This LAI, based on VIs, was assumed as a proxy of the effective LAI. The findings show that the LAI values obtained with the "default" model (using values and thresholds obtained from the literature) have a good agreement with LAI retrieval from satellite measurements, despite a better relationship can be reached with a "model-adjusted" condition. For both scenarios, however, LAI reached approximate maximum values. This demonstrates that, by adopting the default configurations, the resulting LAI development curve will not provide an accurate representation of real conditions. Thus, further experiments are needed to obtain a better representation for the LAI curve development and, hence, may use it as the default mode.

Regarding the LAI retrieval, a considerable increment in the LAI from PS was observed at the end of dormancy probably, which is probably associated with rainfall events that were not estimated in the model due to its boundary conditions (LAI only starts to increase in October). Thus, improvements should be implemented for this component. On the other hand, LAI retrieved from PS showed high oscillations in the growth cycle as well as in the dormant period. It is quite uncertain to affirm what caused these oscillations (uncertainties in satellite reflectance data or uncertainties related to *in situ* measurements), but improvements on the retrieval accuracy are expected for future studies, when larger ground samplings may be conducted. Moreover, the absence of a larger number of UVA samples precluded to make a correlation between the LAI retrieved from both sensors (MAPIR and PS) at this time.

The results of the study show that the model, after some adjustments, can become a powerful tool for bahiagrass LAI simulation and, consequently, for plant development. In

addition, the tests reported in this paper demonstrated that bahiagrass LAI could be estimated through the inversion of EVI2 with reasonable accuracy.

3.6. ACKNOWLEDGMENT

3.7. REFERENCES

ASRAR, G.; FUCHS, M.; KANEMASU, E. T.; HATIIELD, J. L. (1984). Estimating absorbed photosynthetic radiation and leaf area index from spectral reflectance in wheat, Agron. 1. 76:300-306. https://doi.org/10.2134/agronj1984.00021962007600020029x.

BERNI, JOSE A.; ZARCO-TEJADA, PABLO J.; SUÁREZ, LOLA; FERERES, ELIAS. (2009). Thermal and narrowband multispectral remote sensing for vegetation monitoring from an unmanned aerial vehicle. IEEE Transactions on geoscience and Remote Sensing, 47(3), 722-738. https://doi.org/10.1109/TGRS.2008.2010457.

BROGE, N. H.; LEBLANC, E. (2001). Comparing prediction power and stability of broadband and hyperspectral vegetation indices for estimation of green leaf area index and canopy chlorophyll density. Remote sensing of environment, 76(2), 156-172. https://doi.org/10.1016/S0034-4257(00)00197-8.

CANON. (2017). Instruction manual. Available online: <http://gdlp01.c-wss.com/gds/8/0300018448/03/EOS_750D_Instruction_Manual_EN.pdf> (accessed on 30 July 2019).

DARVISHZADEH, Roshanak; ATZBERGER, Clement; SKIDMORE, Andrew; SCHLERF, Martin. (2011). Mapping grassland leaf area index with airborne hyperspectral imagery: A comparison study of statistical approaches and inversion of radiative transfer models. ISPRS Journal of Photogrammetry and Remote Sensing, 66(6), 894-906. https://doi.org/10.1016/j.isprsjprs.2011.09.013.

DAUGHTRY, Craig S. T.; WALTHALL, C. L.; KIM, M. S.; DE COLSTOUN, E. B.; MCMURTREY III, J. E. (2000). Estimating corn leaf chlorophyll concentration from leaf and canopy reflectance. Remote sensing of Environment, 74(2), 229-239. https://doi.org/10.1016/S0034-4257(00)00113-9.

ELVIDGE, Christopher D.; CHEN, Zhikang. (1995). Comparison of broad-band and narrowband red and near-infrared vegetation indices. Remote Sensing of the Environment, 54, 38-48. https://doi.org/10.1016/0034-4257(95)00132-K.

GITELSON, Anatoly A.; MERZLYAK, Mark N.; LICHTENTHALER, Hartmut K. (1996). Detection of red edge position and chlorophyll content by reflectance measurements near 700 nm. Journal of plant physiology, 148(3-4), 501-508. https://doi.org/10.1016/S0176-1617(96)80285-9.

GOBRON, Nadine; PINTY, Bernard; VERSTRAETE, Michel; GOVAERTS, Yves. (1999). The MERIS Global Vegetation Index (MGVI): description and preliminary application. International Journal of Remote Sensing, 20(9), 1917-1927. https://doi.org/10.1080/014311699212542.

GOWER, Stith T.; KUCHARIK, Chris J.; NORMAN, John M. (1999). Direct and indirect estimation of leaf area index, fAPAR, and net primary production of terrestrial ecosystems. Remote sensing of environment, 70(1), 29-51. https://doi.org/10.1016/S0034-4257(99)00056-5.

HALL, F. G.; HUEMMRICH, K.; GOETZ, S.; SELLERS, P; NICKESON, J. (1992) Satellite remote sensing of surface energy balance: success, failures and unresolved issues in FIFE. J Geophys Res 97:19061–19090. https://doi.org/10.1029/92JD02189.

HALL, F. G.; SELLERS, P. J. (1995). First International Satellite Land Surface Climatology Project (ISLSCP) field experiment (FIFE) in 1995. J Geophys Res 100:25,383–25395. https://doi.org/10.1029/95JD03300.

HATFIELD, J. L.; ASRAR, G.; KANEMASU, E. T. (1984). Intercepted photosynthetically active radiation estimated by spectral reflectance, Remote Sens. Environ. 14:65-75. https://doi.org/10.1016/0034-4257(84)90008-7.

HOUBORG, Rasmus; MCCABE, Matthew F. (2018). A cubesat enabled spatio-temporal enhancement method (cestem) utilizing planet, landsat and modis data. Remote sensing of environment, 209, 211-226. https://doi.org/10.1016/j.rse.2018.02.067.

HUETE, A. R. (1988). A soil-adjusted vegetation index (SAVI). Remote sensing of environment, 25(3), 295-309. https://doi.org/10.1016/0034-4257(88)90106-X.

HUETE, A. R.; JACKSON, R. D.; POST, D. F. (1985). Spectral response of a plant canopy with different soil backgrounds. Remote sensing of environment, 17(1), 37-53. https://doi.org/10.1016/0034-4257(85)90111-7.

HUETE, A.; DIDAN, K.; MIURA, T.; RODRIGUEZ, E. P.; GAO, X.; FERREIRA, L. G. (2002). Overview of the radiometric and biophysical performance of the MODIS vegetation indices. Remote sensing of environment, 83(1-2), 195-213. https://doi.org/10.1016/S0034-4257(02)00096-2.

JIANG, Zhangyan; HUETE, Alfredo R.; DIDAN, Kamel; MIURA, Tomoaki. (2008). Development of a two-band enhanced vegetation index without a blue band. Remote sensing of Environment, 112(10), 3833-3845. https://doi.org/10.1016/j.rse.2008.06.006.

JOUVEN, M.; CARRÈRE, P.; BAUMONT, R. (2006). Model predicting dynamics of biomass, structure and digestibility of herbage in managed permanent pastures. 1. Model description. Grass Forage Sci. 61 (2), 112–124. https://doi.org/10.1111/j.1365-2494.2006.00515.x.

KINIRY, J. R., BURSON, B. L.; EVERS, G. W.; WILLIAMS, J. R.; SANCHEZ, H.; WADE, C.; FEATHERSTON, J. W.; GREENWADE, J. (2007). Coastal bermudagrass, bahiagrass, and native range simulation at diverse sites in Texas. Agronomy Journal 99, no. 2, 2007: 450-461. https://doi.org/10.2134/agronj2006.0119.

KROSS, Angela; MCNAIRN, Heather; LAPEN, David; SUNOHARA, Mark; CHAMPAGNE, Catherine. (2015). Assessment of RapidEye vegetation indices for estimation of leaf area index and biomass in corn and soybean crops. International Journal of Applied Earth Observation and Geoinformation, 34, 235-248. https://doi.org/10.1016/j.jag.2014.08.002.

LIU, Jiangui; PATTEY, Elizabeth; ADMIRAL, Stuart. (2013). Assessment of in situ crop LAI measurement using unidirectional view digital photography. Agricultural and Forest Meteorology, 169, 25-34. https://doi.org/10.1016/j.agrformet.2012.10.009.

MAPIR. MAPIR Camera Control (MCC). 2019. Available online: <https://www.mapir.camera/products/mapir-camera-control> (accessed on 31 July 2019).

MAPIR. Mapir Survey 3 Camera. 2018. Available online: <https://www.mapir.camera/collections/survey3/products/survey3n-camera-red-green-nir-rgn-ndvi> (accessed on 25 July 2019).

MARTIN, Thomas Newton; MARCHESE, José Abramo; DE SOUSA, Ana Karenina Fernandes; CURTI, Gilberto Luiz; FOGOLARI, Hoilson; CUNHA, Vinícius dos Santos. Using the ImageJ software to estimate leaf area in bean crop. *Interciencia 38*, no. 12 (2013): 843-848.

MONTEITH, John Lennox. (1977). Climate and the efficiency of crop production in Britain. Philosophical Transactions of the Royal Society of London B 281, 277–294. https://doi.org/10.1098/rstb.1977.0140.

MYNENI, R. B.; WILLIAMS, D. L. (1994). On the relationship between FAPAR and NDVI. Remote Sensing of Environment, 49(3), 200-211. https://doi.org/10.1016/0034-4257(94)90016-7.

NEITSCH, S. L.; ARNOLD, J. G.; KINIRY, J. R.; WILLIAMS, J. R. (2011). Soil and water assessment tool theoretical documentation version 2009. Texas water resources institute. Texas AgriLife Research and USDA Agricultural Research Service, Temple, Texas, USA.

PLANET. (2019). Planet Imagery Product Specification. Available online: <https://assets.planet.com/docs/combined-imagery-product-spec-final-may-2019.pdf> (accessed on 20 July 2019).

ROUSE, J. W.; HAAS, R. H.; SCHELL, J. A.; DEERING, D. W. (1974). Monitoring vegetation system in the great plains with ERTS. Proceedings of the Third Earth Resources Technology Satellite-1 Symposium, Greenbelt, USA; NASA SP-351, 1974; pp. 3010-3017

SCHAPENDONK, A. H. C. M.; STOL, W.; VAN KRAALINGEN, D. W. G.; BOUMAN, B. A. M. (1998). LINGRA, a sink/source model to simulate grassland productivity in Europe.

European Journal of Agronomy, 9(2-3), 87-100. https://doi.org/10.1016/S1161-0301(98)00027-6.

SCHINDELIN, Johannes; ARGANDA-CARRERAS, Ignacio; FRISE, Erwin; KAYNIG, Verena; LONGAIR, Mark; PIETZSCH, Tobias; PREIBISCH, Stephan; RUEDEN, Curtis; Saalfeld, Stephan; Schmid, Benjamin; Tinevez, Jean-Yves; White, Daniel James; HARTENSTEIN, Volker; ELICEIRI, Kevin; TOMANCAK, Pavel; CARDONA, Albert. (2012). Fiji: an open-source platform for biological-image analysis. Nature methods, 9(7), 676.

SELLERS, P. J. (1985). Canopy reflectance, photosynthesis and transpiration, Int. 1. Remote Sens. 6:1335-1372. http://dx.doi.org/10.1080/01431168508948283.

TOWERS, Pedro C.; STREVER, Albert; POBLETE-ECHEVERRÍA, Carlos (2019). Comparison of Vegetation Indices for Leaf Area Index Estimation in Vertical Shoot Positioned Vine Canopies with and without Grenbiule Hail-Protection Netting. Remote Sensing, 11(9), 1073. https://doi.org/10.3390/rs11091073.

TUCKER, Compton J. (1979). Red and photographic infrared linear combinations for monitoring vegetation. Remote sensing of Environment, 8(2), 127-150. https://doi.org/10.1016/0034-4257(79)90013-0.

WILLIAMS, J. R.; JONES, C. A.; KINIRY, J. R.; SPANEL, D. A. (1989). The EPIC crop growth model. Transactions of the ASAE, 32(2), 497-0511. https://doi.org/10.13031/2013.31032.

XIE, Qiaoyun; HUANG, Wenjiang; LIANG, Dong; CHEN, Pengfei; WU, Chaoyang; YANG, Guijun; ZHANG, Jingcheng; HUANG, Linsheng; ZHANG, Dongyan. (2014). Leaf area index estimation using vegetation indices derived from airborne hyperspectral images in winter wheat. IEEE Journal of Selected Topics in Applied Earth Observations and Remote Sensing, 7(8), 3586-3594. https://doi.org/10.1109/JSTARS.2014.2342291.

ZHU, Zaichun; BI, Jian; PAN, Yaozhong; GANGULY, Sangram; ANAV, Alessandro; XU, Liang; SAMANTA, Arindam; PIAO, Shilong; NEMANI, Ramakrishna R.; MYNENI, Ranga B. (2013). Global data sets of vegetation leaf area index (LAI) 3g and fraction of photosynthetically active radiation (FPAR) 3g derived from global inventory modeling and mapping studies (GIMMS) normalized difference vegetation index (NDVI3g) for the period 1981 to 2011. Remote sensing, 5(2), 927-948. https://doi.org/10.3390/rs5020927.

4. CONSIDERAÇÕES FINAIS

A qualidade de vida da população urbana está diretamente relacionada com a existência de áreas verdes, sejam elas pública ou privada, pois elas não apenas oferecem imprescindível serviços ecossistêmicos, mas também valorosos serviços sociais e psicológicos para a manutenção do bem-estar dos residentes urbanos. Portanto, a gestão adequada dessas áreas verdes é de suma importância. Nesse contexto, este estudo teve como objetivo desenvolver um modelo de crescimento de gramíneas para áreas urbanas, especificamente gramados, parques e praças públicas, e beiras de ruas, estradas e corpos d'água. Além disso, o modelo foi desenvolvido para ser integrado em ambiente SIG, o que poderá facilitar, no futuro, a gestão do ambiente citadino pelo poder público, otimizando o sistema de corte de gramíneas.

Os resultados obtidos indicaram que o modelo, implementado a partir de modelos agrícolas pré-existentes (EPIC, ALMANAC e o modelo de JOUVEN), apresentou desempenho considerável nas simulações para o ambiente urbano e demonstra ser uma feramente de auxílio promissora na gestão de poda e controle paisagístico de gramíneas.

No contexto da implementação do modelo, ao contrário do que acontece no setor agrícola, não há o controle de nutrientes no solo em áreas urbanas pelo poder púbico e, consequentemente, não se pratica a adição de fertilizantes. Assim, o modelo incorporou apenas os parâmetros temperatura, teor de água no solo e radiação solar como inibidores do crescimento da planta. Dentre os três parâmetros inibidores do crescimento, o teor de água no solo se mostrou ser o fator de maior impacto. Deste modo, o modelo proposto traz duas abordagens para o cálculo do estresse hídrico: (i) a dinâmica da quantidade de água infiltrada e retirada pela planta e (ii) o índice de terreno, o qual é considerado nesse trabalho uma estimativa da taxa de escoamento subterrâneo. Não foram encontrados registros na literatura de sistemas utilizando as duas abordagens no campo da modelagem do crescimento da vegetação, cuja integração se mostrou consistente, conforme observado nos resultados alcançados.

A adaptação do modelo para ambiente SIG se dá a partir do mapeamento das áreas verdes urbanas de responsabilidade do poder público e, uma vez que o mapeamento seja concluído, as áreas são incorporadas ao modelo. O modelo simula o crescimento da vegetação

para cada área de forma independente, considerando as suas características e o seu regime de corte. Isso permite que áreas com maior necessidade de poda sejam identificadas e priorizadas.

O modelo ainda apresenta dois estágios de desenvolvimento da planta, período de crescimento e dormência. Na dormência, o modelo apresenta um decaimento sigmoide ao invés de linear (comum na maioria dos modelos existentes), o que representa uma maior fidelidade ao observado em campo. Entretanto, observou-se que a grama batatais (*Paspalum notatum* Flügge) apresentou um pequeno crescimento no período que foi classificado como dormente. Assim, ajustes para esse parâmetro ainda precisam ser executados.

Dessa forma, o modelo proposto nesse trabalho pode ser considerado uma ferramenta promissora de subsídio para a gestão apropriada de áreas verdes urbanas (compostas por gramíneas) quanto ao regime de corte e controle paisagístico. O modelo permite o acompanhamento diário da dinâmica do desenvolvimento da grama de cada área verde mapeada por meio da visualização da dinâmica do IAF. Dessa forma, uma vez que se tem o monitoramento do IAF, espera-se que haja uma otimização do processo de corte (i.e., identificação dos momentos mais apropriados para a sua aplicação do corte), o que por sua vez, significaria uma redução dos custos relacionados à essa prática.

Quanto a trabalhos futuros e levando-se em consideração que o IAF recuperado por meio do VIs são uma representação do índice de área foliar efetivo, recomenda-se: (i) ajustes na curva de desenvolvimento do índice de área foliar (IAF), os quais devem ser incorporados às configurações padrão do modelo, (ii) adequações no estágio de dormência, e (iii) número amostral *in situ* maior do que o realizado nesse trabalho ($n = 11$), sobretudo amostras com IAF inferior a 1 ou superior a 2.